PHYSICS REPORTS (Review Section of Physics Letters) 154, No. 2 (1987) 77–123. North-Holland, Amsterdam

RELEVANCE OF CLASSICAL CHAOS IN QUANTUM MECHANICS: THE HYDROGEN ATOM IN A MONOCHROMATIC FIELD

Giulio CASATI[a]

Dipartimento di Fisica dell'Universita, Via Celoria, 16-20133 Milano, Italy

Boris V. CHIRIKOV and Dimitri L. SHEPELYANSKY

Institute of Nuclear Physics, 630090 Novosibirsk, USSR

and

Italo GUARNERI[b]

Dipartimento di Fisica Teorica e Nucleare, Universita di Pavia, 27100 Pavia, Italy

Received March 1987

Contents:

1. Introduction 79
2. Semiclassical theory of electron excitation 81
   2.1. Classical dynamics of electron excitation 81
   2.2. Theory of quantum localization 85
   2.3. Ionization in the presence of localization 89
   2.4. Comparison of diffusive and one-photon ionization 90
   2.5. Ionization by tunneling and Keldysh parameter 91
3. Numerical results 93
   3.1. Methods of numerical simulation 93
   3.2. Numerical results on the classical model 100
   3.3. The distribution over the unperturbed levels 101
   3.4. Dependence of the excitation probability on frequency 110
   3.5. Stability of quantum diffusion 114
4. Experimental results 115
5. Conclusions 116
Appendix I: Quasi-classical matrix elements in parabolic coordinates 118
Appendix II: Solution of the Fokker–Planck equation 119
Appendix III: Estimate for the delocalization border 121
Appendix IV: A method for computing hypergeometric functions 121
References 122

(a) Also at Istituto Nazionale di Fisica Nucleare, Sezione di Milano, Milano, Italy.
(b) Also at Istituto Nazionale di Fisica Nucleare, Sezione di Pavia, Pavia, Italy.

Single orders for this issue

PHYSICS REPORTS (Review Section of Physics Letters) 154, No. 2 (1987) 77–123.

Copies of this issue may be obtained at the price given below. All orders should be sent directly to the Publisher. Orders must be accompanied by check.

Single issue price Dfl. 34.00, postage included.

0 370-1573/87/$16.45

RELEVANCE OF CLASSICAL CHAOS IN QUANTUM MECHANICS: THE HYDROGEN ATOM IN A MONOCHROMATIC FIELD

Giulio CASATI

Dipartimento di Fisica dell'Universita, Via Celoria, 16-20133 Milano, Italy

Boris V. CHIRIKOV and Dimitri L. SHEPELYANSKY

Institute of Nuclear Physics, 630090 Novosibirsk, USSR

and

Italo GUARNERI

Dipartimento di Fisica Teorica e Nucleare, Universita di Pavia, 27100 Pavia, Italy

NORTH-HOLLAND—AMSTERDAM

Abstract:

We present analytical and numerical results on the mechanism of excitation and ionization of hydrogen atoms under microwave fields. In particular we predict the existence of a critical value of the microwave field, *the quantum delocalization border*, above which the quantum packet delocalizes and strong excitation and ionization takes place. Below the quantum border, the packet is localized even though the corresponding classical system can be chaotic and obeys a diffusion equation.

Our studies reveal some other unexpected new features of quantum dynamics which also could be observed in laboratory experiments and provides a quantum theory for subthreshold ionization.

1. Introduction

In the last years significant interest has been devoted to quantum systems that are chaotic in the classical limit [1–3]. It has by now become clear that such systems display quantum dynamical properties that, even in the quasi-classical region, may be very different from the classical ones.

In our opinion, the most interesting phenomenon discovered in this connection is the quantum limitation of the classical chaotic diffusion. This phenomenon was first observed in numerical experiments on the periodically kicked quantum rotator [4]. The classical limit of this system exhibits a "stochastic transition" for a certain value of the perturbation strength [5]. Above this value, the system behaves in a quite disordered way, its motion being almost the same as if the perturbation were a random and not a deterministic one. In particular, its energy grows indefinitely, according to a diffusive law.

In the corresponding quantum system this chaotic diffusion is suppressed. Strictly speaking, the quantum dynamics of the rotator depends in a sensitive way on the arithmetic relationship between the rotator and the external frequency [12]. Nevertheless, apart for an exceptional set of values of this frequency ratio, quantum interference effects lead to a complete arrest of the diffusive growth of energy after a finite time. As a result, only a finite number of unperturbed levels are significantly excited during the whole course of quantum evolution [3, 4, 6, 7].

This quantum limitation of chaos may be considered as a dynamical version of the Anderson localization in one-dimensional disordered solids [8]. For the rotator problem, the localization length was shown to be equal to the classical diffusion rate, up to some numerical factor [9–11], and this by the way, may help to solve some new problems in solid state physics too.

Even though the quantum suppression of chaos was mainly investigated on the very particular rotator model, nonetheless the nature of the arguments supporting it, and especially the localization picture, indicate that quantum mechanics should indeed have an inhibitory effect on classical chaos even for generic quantum systems subject to time-periodic perturbations. This is in itself a remarkable discovery, bringing into light once more the deep fundamental difference between quantum and classical mechanics.

However, there are sound reasons to believe that this quantum suppression of chaos must suffer significant exceptions. As a matter of fact, the existence of a kind of quantum motion retaining some features of classical chaotic diffusion is at the present time the only possible explanation for available experimental results on the ionization of highly excited H-atoms (principal quantum number $n \sim 60$) in microwave fields of frequency $\omega/2\pi \sim 10\,\text{GHz}$ with peak intensity $\varepsilon \sim 10\,\text{V/cm}$, in conditions where ionization would require the absorption of ~100 photons [13, 14].

In order to explain the surprising high ionization probability observed in experiments, a diffusive excitation mechanism was suggested in [15], while, in [16], it was pointed out that a classical description might be appropriate due to the high quantum numbers involved. Indeed, a numerical solution of the

classical equations of motion [16] yields a satisfactory agreement with experimental data [13]. In the classical system ionization is brought about by the chaotic motion of the electron, which causes diffusive excitation for field strength above some critical value [17]. The conditions under which this chaotic excitation occurs and the related diffusion rate were obtained [18, 20] by means of the resonance overlap criterion [5]. At this point, a most important question was how quantum effects would modify this classical picture of diffusive excitation, since, in view of the results on the quantum rotator, hinted to above, one may expect some quantum limitation of classical diffusion to occur in the H-atom, too.

In order to answer this question, a model for the hydrogen atom in a microwave field, that can be solved at least numerically, both classically and quantum mechanically is needed. One such model is indeed available: it describes the one-dimensional motion of an electron in a Coulomb field plus an external monochromatic electric field. As discussed in [19], and as we will recall in the present paper, this model conveniently describes an actual H-atom prepared in a so-called extended state. The same one-dimensional model can be used in order to describe excitation of surface state electrons on liquid helium [20, 21].

The present paper is devoted to a detailed study of this one-dimensional model, including a large amount of numerical data and the theoretical framework developed in order to interpret them. Some of these results we already presented in previous short papers [19, 22, 46, 47] and also much of the theoretical analysis presented here, appeared before in a more or less fragmented way. Here we attempt at a systematic exposition, including details of the numerical techniques. Besides that, we also present many fresh numerical data, obtained by a numerical method especially devised in order to take into account the continuous part of the unperturbed spectrum.

Indications from these and older results merge into a definite picture according to which quantum effects do indeed produce a quantum limitation of chaos in this problem, so that it is possible to observe situations where the quantum packet is localized in contrast to the chaotic diffusion that would be predicted by classical mechanics. Nevertheless, it was possible to identify a critical value for the field strength, typically lying above the classical chaotic threshold, above which a "diffusive" excitation takes place in the quantum atom, too. In this region the classically predicted ionization rate is a good approximation to the real quantum rate. An unexpected consequence of this fact is the existence of a frequency threshold for ionization, lying well below the conventional photoelectric threshold for 1-photon ionization, and leading to a much stronger ionization than predicted by the standard perturbative theory of the photoeffect.

Another interesting phenomenon discussed in some detail here is the appearance of peaks in the distribution connected with multiphoton transitions over the unperturbed levels.

On the theoretical side, we give here conditions for the applicability of the one-dimensional approximation both in the classical and in the quantum case, and we explain the estimate presented in [22] for the two-dimensional delocalization border, which is much lower than in the one-dimensional case. We also give a theoretical prediction for the ionization probability over long interaction times, and for its dependence on the field strength, for a given initial distribution of the atoms over the quantum states with a given principal number.

Experimental techniques are nowadays available, that allow for laboratory investigations on highly excited atoms; see, e.g., [13, 14, 23–27]. It is even possible to prepare atoms with prescribed parabolic quantum numbers; for instance, in [24] extended states with parabolic number $n_1 = 0$ and magnetic number $m = 0$ were prepared, and it was shown that one-dimensionality is preserved during the interaction time. Therefore, the one-dimensional model is appropriate. On the other hand, in these experiments the perturbing microwave field was well below the threshold for the classically chaotic

motion [28], and they do not therefore allow us to decide whether classical chaos survives in quantum mechanics.

Recent experiments [27] on three-dimensional atoms with $\omega n^3 \approx \frac{1}{2}$ have shown that the critical field strength, required for strong excitation, is close to the value for which chaotic excitation takes place in the classical atom. These experiments therefore demonstrate an agreement between quantum and classical chaotic excitation. According to our numerical computations these experiments were made in the delocalization regime, so that this result is consistent with our theoretical predictions, too.

In order to observe in laboratory experiments the phenomenon of quantum localization, which is predicted and explained in this paper both on numerical and on theoretical grounds, it is necessary to prepare atoms in extended states and to go to the high frequency region ($\omega n^3 > 1$) in which this phenomenon should be particularly clear. Such experimental verification of the localization phenomenon seems to lie within the scope of present experimental techniques.

The theory we present here is certainly still in a very primitive stage, and great improvements are needed in order that the role of classical Chaos in Quantum Mechanics be completely clarified. However, we believe that all the physically essential traits are already present in our provisional analysis. In particular, we believe that semiclassical arguments cannot be dispensed with in any attempt to expose diffusive-like excitation mechanism in the quantum H-atom.

2. Semiclassical theory of electron excitation

2.1. Classical dynamics of electron excitation

In this section we will develop the classical theory of the excitation of a hydrogen atom in a linearly polarized monochromatic electric field.

Here and in the following we will use atomic units, in which the Hamiltonian takes the form:

$$H = p^2/2 - 1/r + \varepsilon z \cos \omega t \tag{1a}$$

where ε and ω are the field strength and frequency respectively and the z-coordinate is measured along the direction of the external field. The classical dynamics associated with (1a) is conveniently studied in parabolic coordinates since the unperturbed dynamics is separable in these coordinates. Accordingly, action-angle variables $(n_1, n_2, m, \lambda_1, \lambda_2, \varphi)$ can be introduced [31], in which the Hamiltonian takes the form:

$$H = -1/2n^2 + \varepsilon\, z(n_1, n_2, m, \lambda_1, \lambda_2) \cos \omega t\,; \qquad n = n_1 + n_2 + |m|\,. \tag{1b}$$

Owing to axial symmetry, m (which is the z-component of the angular momentum) is an integral of the motion; therefore, (1) describes an essentially two-dimensional model.

The function $z(n_1, n_2, m, \lambda_1, \lambda_2)$ can be expanded in a double Fourier series in the angle variables λ_1, λ_2:

$$z = \sum_{k_1 k_2} z_{k_1 k_2}(n_1, n_2, m) \exp\{\mathrm{i}(k_1 \lambda_1 + k_2 \lambda_2)\}\,. \tag{1c}$$

The coefficients $z_{k_1 k_2}$ can be found as shown in appendix I, and are given by [19]:

$$z_{k_1k_2} = [n^2/(k_1+k_2)]\,[\mu_2\, J_{k_1}(\mu_1(k_1+k_2))\, J'_{k_2}(\mu_2(k_1+k_2)) - \mu_1\, J'_{k_1}(\mu_1(k_1+k_2))\, J_{k_2}(\mu_2(k_1+k_2))]\,; \qquad \text{for } k_1+k_2 \neq 0$$
$$z_{k,-k} = \begin{cases} 0 & \text{for } k \neq 0 \\ 3n(n_1-n_2)/2 & \text{for } k = 0\,. \end{cases} \tag{1d}$$

Here J_k are Bessel functions of the first kind and J'_k their derivatives. The dependence of $z_{k_1k_2}$ on n_1, n_2, m is embodied in the parameters μ_1, μ_2, which are defined by

$$\mu_{1,2} = (n_{1,2})^{1/2}(n_{1,2}+|m|)^{1/2}/n\,. \tag{1e}$$

According to standard semiclassical approximation theory [29], $z_{k_1k_2}$ give semiclassical values of dipole matrix elements for the transitions $n_{1,2} \to n'_{1,2} = n_{1,2} + k_{1,2}$. The element $z_{0,0}$, which is just the average of z over the unperturbed torus labelled by n_1, n_2, m, yields the standard quantum mechanical expression for the linear Stark effect.

If the electron is initially in an "almost one-dimensional" state, i.e., in a state with $n_1 \gg n_2$, $n_1 \gg m$, then in (1a–1e) we can assume $\mu_1 = 1$, $\mu_2 = 0$. In that case, the dynamics will be described in first approximation by the one-dimensional Hamiltonian

$$H = -1/2n^2 + \varepsilon n^2 \cos\omega t \left[\tfrac{3}{2} - 2\sum_{k=1}^{\infty} J'_k(k)\, k^{-1} \cos k\lambda\right] \tag{2}$$

which is just the Hamiltonian, in action-angle variables, for an electron moving along the positive z-axis [18, 21]:

$$H = p^2/2 - 1/z + \varepsilon z \cos\omega t\,, \qquad z > 0\,. \tag{2a}$$

We start our analysis with this simplified Hamiltonian (2). Later in this section we shall discuss the validity of this one-dimensional approximation, i.e. we shall discuss to what extent the one-dimensional Hamiltonian (2) is adequate in order to describe the evolution of quasi-one-dimensional initial states under the full Hamiltonian (1).

Under appropriate conditions, the classical system described by the Hamiltonian (2) undergoes a transition to chaotic dynamics. By this we mean that a profound change occurs in the nature of orbits, which, above a certain perturbation strength, become extremely sensitive and complicated and wander erratically in phase space. This irregular motion, if described in the unperturbed action–angle space, has a diffusive character and leads to fast ionization. Quantitative conditions for the onset of chaotic dynamics can be obtained by means of the resonance overlapping criterion [18, 21]. The starting point of this analysis is realizing that the external field will more effectively perturb the undisturbed motion at first-order resonances, i.e., at values n of the unperturbed actions such that the external frequency ω resonates with some harmonic of the unperturbed electron motion. These values of n are such that $s\,\Omega(n) = \omega$ with s an integer and $\Omega(n)$ the angular frequency (Kepler frequency) of the unperturbed motion:

$$\Omega(n) = \mathrm{d}H_0/\mathrm{d}n = 1/n^3\,.$$

First-order resonances are then given by $n_s = (s\omega^{-1})^{1/3}$. However, despite the fact that for these

values n_s the perturbation is very effective, as soon as it manages to drive the motion away from one unperturbed resonant orbit its effect becomes weaker, and nonlinear stabilization may occur. In that case, the motion remains in a neighborhood (a "resonance region") of the original unperturbed orbit.

However, if the perturbation is sufficiently strong, the motion can be driven so far away from the original resonant value of the action, that it can fall under the influence of another nearby resonance. There, the same process may repeat, so that the orbit may wander in action–angle space in a diffusive way.

A quantitative estimate of the perturbation strength which is necessary in order that this may happen is determined by evaluating the width of the various resonance regions and then by requiring that nearby regions overlap [18].

The analysis just outlined can be applied to model (2); it is then found that for $\omega_0 = \omega n_0^3 > 1$ (where n_0 is the initial value of the action) and for field strength exceeding a critical value ε_{cr}

$$\varepsilon_0 = \varepsilon n_0^4 > \varepsilon_{cr} \sim 1/(50\omega_0^{1/3}) \tag{3}$$

all resonance regions corresponding to $n_s \geq n_0$ do overlap. Then an orbit leaving with action n_0 in a region of phase space where both $\omega_0 > 1$ and (3) are satisfied will diffuse indefinitely and eventually ionize.

Notice that in (3) we have introduced rescaled values $\varepsilon_0 = \varepsilon n_0^4$ for field and $\omega_0 = \omega n_0^3$ for frequency. The usefulness of this scaling is due to the fact that classical dynamics depends on n_0 only via these variables since, as can be readily checked, changing the initial n_0 by some factor will change the solution $n(t)$ at any later time by the same factor, provided ε_0 and ω_0 are kept constant, and time is measured in periods of the field (see also [16]).

We emphasize that the estimate (3) is valid only for $\omega_0 > 1$. Indeed for $\omega_0 < 1$, i.e. in that phase space region where ω is smaller than the Kepler frequency, there are no first-order resonant values of n, and the motion is therefore more stable. A transition to chaotic behavior can still occur [18, 21] due to the finite width of the resonance region associated with $\omega_0 = 1$, but, in order to compute the ε_{cr} in this region, also higher-order resonances $s\Omega = p\omega$, $p > 1$ must be taken into account. It is then found that the critical field increases with decreasing ω_0; however, for very low ω_0 static field ionization occurs when $\varepsilon_0 \approx 0.13$.

Of course, higher-order resonances play a role in the chaotic transition also for $\omega_0 > 1$ and, indeed, an approximate account of them was already taken in (3) via the choice of the numerical factor 1/50 [18]. A proper second-order analysis [30] leads to but a small increase in this numerical factor.

In the chaotic regime, $\varepsilon_0 > \varepsilon_{cr}$, $\omega_0 > 1$ the process of diffusive excitation is conveniently described in statistical terms. Indeed, an equation of the Fokker–Planck type can be derived [18]:

$$\partial f/\partial \tau = \tfrac{1}{2}\, \partial/\partial n (D\, \partial f/\partial n) \tag{4}$$

where $f(n, \tau)$ is the distribution and τ is the dimensionless time, measured as the number of periods $\tau = \omega t/2\pi$ of the external field. The diffusion coefficient D in quasi-linear approximation is given by

$$D = \mathrm{d}\langle(\delta n)^2\rangle/\mathrm{d}\tau \approx 2\varepsilon_0^2 n^3/(\omega_0^{7/3} n_0) = 2\varepsilon^2 n^3/\omega^{7/3} \tag{5}$$

((4) and (5) were also derived in [21]).*

* The numerical coefficient 2 in (5) corresponds to the frequency range $1 < \omega_0 < 3$. For $\omega_0 \gg 3$, the asymptotic value of this coefficient must be used, which is near to 3.

Since D increases with n according to a power law, it is possible to find an exact solution of (4). In order to do this, we must take notice that the stochastic diffusion ruled by (4) can take place only in that part of phase space where the chaotic transition has occurred. Going down to lower and lower action values, one will eventually meet an invariant curve which has not been destroyed; we must therefore look for a solution of (4) satisfying the boundary condition $\partial f/\partial n|_{n=n^*} = 0$ of zero flux across the boundary $n = n^*$ of the region of stability. In order to do that, the change of variables $y = n/n_0$, $\bar{\tau} = \tau\varepsilon_0^2\omega_0^{-7/3}$ is convenient. Then, as shown in appendix II, for $\bar{\tau}\sqrt{\bar{y}} \ll 1$ and letting $\bar{y} = n^*/n_0$, the solution assumes a sufficiently simple form:

$$f(y, \bar{\tau}) \approx \{\exp[-(1/\sqrt{y} - 2/\sqrt{\bar{y}} + 1)^2/\bar{\tau}] + \exp[-(1/\sqrt{y} - 1)^2/\bar{\tau}]\}/[2y^{3/4}(\pi\bar{\tau})^{1/2}]\,. \tag{5a}$$

As will be seen in section 3, this formula compares remarkably well with the results of numerical integration of the equations of motion.

The possibility of using this statistical description will play an important role in our subsequent analysis of the ionization process. Indeed, due to the rapid growth with n of the diffusion coefficient, stochastic orbits diffuse so fast towards high values of n that in practice we can assume that they actually ionize – i.e. n becomes infinite – in a finite time. A rough estimate of the ionization time adequate for our present purposes can be gotten from eq. (5) (see also eq. (12)):

$$\tau_I \sim n_0^2/D \sim \omega_0^{7/3}/(2\varepsilon_0^2)\,. \tag{6}$$

In later sections we'll use expression (6) in order to roughly estimate the diffusive ionization rate $P_I \sim \tau_I^{-1}$.

In the remainder of this section we discuss the validity of the one-dimensional approximation (2). Let's consider first the case when $n_1 \gg n_2$, $n_1 \gg m$ and therefore $\mu_2 \ll 1$. Then, since $z_{k_1k_2} \sim \mu_2^{|k_2|}$ for large $|k_2|$, the main contribution to the variation of n_2 will be given by terms in (1c,d) with $k_2 = \pm 1$. (Notice that $z_{k_1k_2}$ give semiclassical matrix elements for transitions with $\Delta n_2 = \pm k_2$. The fast decrease of these matrix elements with small μ_2 when k_2 is large was already remarked in [32].)

For $\varepsilon_0 > \varepsilon_{cr}$, the phase λ_1 begins to vary chaotically, and this leads to a diffusive change in n_2 also. The diffusion rate for n_2 in quasi-linear approximation can be derived, as shown in [17], by retaining in (1c) only terms with $k_2 = \pm 1$. One finds that:

$$D_2 \approx n_2(n_2 + |m|)D/n^2\,. \tag{7}$$

This estimate shows that over the ionization time (6) the change in n_2: $(\Delta n_2)^2 \sim n_2\,(n_2 + |m|) \ll n^2$ appears to be small. This fact indicates that the onset of stochasticity doesn't lead to significant violations of the one-dimensional approximation.

Along similar lines, we can show that a suitable one-dimensional approximation is valid also in cases when $n_1 \sim |m| \gg n_2$. Indeed from (1e) it follows that, in such cases also, $\mu_2 \ll 1$. Then, upon neglecting μ_2 in (1c,d) we obtain the one-dimensional dynamics for the variable $n_1 = n - |m|$, described by the Hamiltonian

$$H = -1/2n^2 + \varepsilon n \cos\omega t\left[3(n - |m|)/2 - 2\mu_1 n \sum_k J_k'(\mu_1 k)\, k^{-1} \cos k\lambda_1\right] \tag{8}$$

with $\mu_1 \approx (1-|m|/n)^{1/2}$. We can now apply to this one-dimensional dynamics the resonance analysis, just as was done for (2). From the asymptotic properties of $J'_k(k\mu_1)$ for $k \to \infty$ [33] it follows that high-k harmonics in (8) become exponentially small as soon as k is so high that $(3/k)^{2/3} \leq m/n$. This means that the resonances of the field with such high harmonics (which take place when $\omega_0 = k$ with $(3/k)^{2/3} \leq m/n$), cannot significantly contribute in the chaotization process. Therefore, when $\omega_0 \gg 1$ the transition to chaotic motion is possible only for $m \lesssim m_{cr}$, with

$$m_{cr} = n_0(3/\omega_0)^{2/3} \qquad \text{for } \omega_0 \gg 1 . \tag{9}$$

For $\omega_0 \sim 1$ we may take $m_{cr} \approx n_0$. At this point we might start afresh the analysis for the Hamiltonian (8) in order to determine the critical field and the diffusion rate under condition (9). However a comparison of (8) with (2) suggests that the results of this analysis shouldn't deviate more than a factor 2 from formulas (4) and (5).

Again, the one-dimensional approximation (8) is not significantly violated over the ionization time; this can be seen at once, because the diffusion rate for n_2 is still given by (7), so that an estimate for the variation Δn_2 similar to the previously established one for (2) holds for the present case.

Further details on the classical dynamics of excitation for the model (2) will be given in section 3.2, where we shall also discuss the results of numerical simulations of this model.

2.2. *Theory of quantum localization*

The main result of the classical analysis carried out in the previous section was that for sufficiently strong fields the classical model (2) exhibits a transition to chaotic motion. After this, the classical distribution $f(n, \tau)$ spreads diffusively in action space, and ionization takes place in a finite time.

We will now tackle the basic question, of what modifications would be imposed on this picture by quantum mechanics. In particular, we will study the behavior of the quantum probability distribution over the unperturbed levels, which is the quantum analog of $f(n, \tau)$.

Previous studies on periodically perturbed quantum systems that become chaotic in the classical limit – in particular, on the kicked rotator model – brought to light the localization phenomenon as a typical occurrence. The quasi-energy spectrum is typically a pure point one, and quantum effects lead to a limitation of the classical diffusion and to exponential localization of the probability distribution around the initially excited level n_0; which means that in the average, and apart from fluctuations (which can be large) the distribution looks like:

$$\bar{f}_n \propto \exp(-2|n-n_0|/l) . \tag{10}$$

Here $\bar{f}_n$ is the time-averaged population over the unperturbed levels with the values n for the quantized actions, and l is the localization length.

In the light of these previous findings, it is natural to assume that a similar picture applies also in the present case. Specifically, we will assume that even in the semiclassical region, and when the classical motion is chaotic, a mechanism of quantum limitation of the chaotic diffusion is working, and that, under suitable conditions, this mechanism will produce a situation analogous to the rotator case. Under such conditions, the part of the q.e. spectrum relevant to our analysis will be quasi-discrete; the small line breadth of its levels will be negligible on a time scale short in comparison with the very long one associated with multiphoton ionization. While it remains true that the quantum atom described by (2)

will eventually ionize, no matter how small ε, nevertheless on the time scale involved in the actual experiments the localization phenomenon discussed here will give it a remarkable stability in contrast with the properties of chaotic motion. The obvious premise that localization in the hydrogen atom is related to a finite time scale, should not be forgotten throughout this paper. This assumption will be fully supported by the results of our numerical experiments.

Under such assumptions, we shall presently determine the localization length by the simple method described in [3]. In this way, we will be able also to determine the quantitative conditions under which the localization picture actually applies. To this end, let us start with the case of homogeneous classical diffusion, that is, we overlook the variation of D with n.

In the semiclassical regime, the evolution of a quantum state initially coinciding with one unperturbed eigenstate n_0 will initially follow to some extent the classical development of $f(n, \tau)$. Therefore, over the time scale in which this semiclassical approximation holds, the spread of the wave packet over the unperturbed eigenstates will grow in time according to $\Delta n(\tau) \approx (D\tau)^{1/2}$.

However, the discrete character of the quasi-energy spectrum will prevent this diffusive growth from going on indefinitely, as it would in the classical case. The time τ_D after which the discreteness of the quasi-energy spectrum will become manifest can be estimated by $\tau_D \sim N$, where N is the number of q.e. eigenstates significantly excited by the original unperturbed eigenstate; indeed $2\pi/N$ is just the average spacing of q.e. eigenvalues significantly contributing to the packet evolution. Then, the number of unperturbed levels excited by the wave packet after the time τ_D is $\Delta n(\tau_D) \approx (D\tau_D)^{1/2}$. This means that one unperturbed level contains $N \sim \Delta n(\tau_D)$ q.e. levels and that, *vice-versa*, one q.e. eigenstate "contains" $\sim \Delta n(\tau_D)$ unperturbed levels. The latter number, however, is the maximum spread attainable by the wave packet, i.e., it coincides with the localization length l. Therefore we get an equation for τ_D:

$$\tau_D \approx \alpha\, \Delta n(\tau_D) \approx \alpha\, (D\tau_D)^{1/2} \approx \alpha l$$

where we have introduced an undetermined numerical factor α, to be found by numerical experiments [10]. For the rotator model, it was found $\alpha \approx 1$. The same choice for α in the hydrogen atom case would yield

$$l \approx D(n_0) \approx \tau_D \tag{11}$$

where $D(n_0)$ is given by (5): $D(n_0) = 2\varepsilon_0^2 n_0^2 \omega_0^{-7/3}$.

However this result was obtained under the assumption that $D \approx$ const., which is justified only in that region where $l \ll n_0$. Instead, for $l \sim n_0$, the dependence of D on n may substantially modify the localization picture, and, if the field strength exceeds some critical value, it may even turn out that localization is not possible at all. (A similar "delocalization" phenomenon was investigated and explained in a simple example in refs. [3, 10].)

In order to clarify how delocalization occurs, we need to modify the above method for determining l, in such a way that the dependence of D on n is explicitly taken into account. Therefore, in place of $\Delta n(\tau) \approx (D(n_0)\,\tau)^{1/2}$ we must substitute the dependence of Δn on τ that is enforced by the Fokker–Planck equation (4). In this way we find, as a result of the calculations developed in appendix III, that $\Delta n(\tau)$ is given by:

$$\Delta n(\tau) = [(1 - 3\varepsilon_0^2 \omega_0^{-7/3} \tau)^{-2} - 1]^{1/2} n_0/\sqrt{3}\,. \tag{12}$$

By the same argument as above, we can now find τ_D and l from the localization condition $\Delta n(\tau_D) = \tau_D$. However, if ε_0 is large enough, the curve $\Delta n(\tau)$ will never intersect the straight line $\alpha\tau$ before exploding at $\tau = \omega_0^{7/3}/3\varepsilon_0^2$. When this happens, no localization is possible and this implies unbounded diffusion for the electron. More specifically, in appendix III we show that the solution of $\Delta n(\tau_D) = \alpha\tau_D$ gives the localization length l in the form:

$$l \approx \alpha^{-1}(\omega_0^{7/3}/\varepsilon_0^2)u/3 \tag{13}$$

where u is the least of the two solutions of the equation*

$$3\alpha^2(\omega_0^{-7/6}n_0^{1/2}\varepsilon_0)^4 = g(u) \equiv u(1-u)^2/(2-u) \tag{14}$$

such that $0 < u < 1$. Numerical data indicate that here too, like in the rotator case, $\alpha \approx 1$ is to be chosen (see e.g. fig. 10 and related comments in section 3). Therefore, since the function $g(u)$ in the interval $(0, 1)$, has a maximum $\approx 1/11$ at $u = (3-\sqrt{5})/2$, it follows that for

$$\varepsilon_0 > \varepsilon_q^{(1)} = \omega_0^{7/6}/\sqrt{6n_0} \tag{15}$$

eq. (14) has no solution.

Thus $\varepsilon_q^{(1)}$ defines the *threshold for quantum delocalization*. Of course, in order that delocalization may occur, it is also necessary that ε_0 exceeds the threshold for classical chaos (3), because the semiclassical estimate (12) holds under the assumption that chaotic diffusion takes place in the classical system. According to the argument just outlined, across the threshold $\varepsilon_q^{(1)}$ a qualitative change occurs, and the localization picture is no longer justified. We should then expect that above this threshold there is no quantum limitation to the classical diffusion and, indeed, this will clearly appear from numerical results.

In deriving the above estimate we implicitly assumed that all unperturbed levels are involved in the diffusion. However, this is true only under the condition (see ref. [36])

$$\varepsilon z_{nn'} > \omega/2$$

where n and n' are such that the associated transition is the "most nonresonant" one, i.e.: $\omega/2 = 1/2n^2 - 1/2n'^2$.

Then since [34]:

$$z_{nn'} \approx 1.3/[\omega^{5/3}(nn')^{3/2}]\,. \tag{15a}$$

We get the following condition:

$$\varepsilon_0 > \omega_0^{8/3}n^3/3n_0^4\,. \tag{15b}$$

In particular, the delocalization estimate (15) holds if $\omega_0 < n_0^{1/3}$ ($n \approx n_0$). Inequality (15b) is always

* The slight difference in numerical coefficients between (13) and the analogous formula of ref. [22] is due to the fact that in [22] a value of α somewhat lesser than 1 was introduced in $l = \alpha D$.

violated for sufficiently high n which results in arising a chain of sharp peaks related to the successive one-photon resonant transitions both in the localization and delocalization regimes (see figs. 7 and 14). Particularly, behind the last peak a formal power law 'localization' builds up [50] due to the decay of the matrix element $z_{nn'}$. However, the ionization is not at all suppressed, and does proceed over the region of 'localization' via a fast direct one-photon transition into continuum.

The above one-dimensional analysis can now be modified, so as to apply also in the two-dimensional case for quasi-one-dimensional states. Indeed, even though we know from section 2.1 that the one-dimensional approximation is not violated for such states, still we cannot *a priori* exclude that the presence of an additional degree of freedom can destroy the localization of these quasi, but not strictly, one-dimensional states. However, we can answer this question by the same method used in the one-dimensional case. Assuming that the classical diffusion proceeds independently in both $n_1 \approx n$ and n_2, the number of unperturbed levels excited at time τ will be ($\Delta n_2 > 1$)

$$N \approx \Delta n_1(\tau)\, \Delta n_2(\tau)\,.$$

For $\Delta n_1(\tau)$ we will now take eq. (12); moreover, since $\Delta n_2(\tau) \ll n_1$ can be assumed (see section 2.1), we will take $\Delta n_2(\tau) \sim (D_2\tau)^{1/2}$ with D_2 as in formula (7). Imposing now the delocalization condition $N \geq \tau$ [3, 6, 10, 11, 19, 22] one easily gets the estimate for the two-dimensional delocalization threshold:

$$\varepsilon_0 > \varepsilon_q^{(2)} = \beta\omega_0^{7/6}/\{n_0[n_2(n_2+|m|)]^{1/2}\}^{1/2} \tag{16}$$

where again an undetermined numerical factor $\beta \sim 1$ was introduced.*

The estimate (16) clearly indicates that two-dimensionality sharply decreases the delocalization threshold. Nonetheless, for states with $m \sim n_2 \sim 1$ the two-dimensional threshold is almost the same as the one-dimensional one. We are therefore justified in assuming that for such quasi-one-dimensional states, the localization–delocalization picture remains valid.

In closing this section, a couple of remarks concerning the validity of considering the quantum system described by the Hamiltonian (2) to be a physically realistic model are in order. In the first place, in the quantum theory discussed above we considered the electric field as classical. This approximation holds if the full number N of field quanta inside the microwave cavity of volume V:

$$N = V\varepsilon^2/(4\pi\hbar\omega) \sim 10^{23}\varepsilon_0^2/(n_0^5\omega_0)$$

is sufficiently large. For instance, for $\varepsilon_0 = 0.05$, $\omega_0 = 1$, $n_0 = 100$, $V = 1\,\mathrm{cm}^3$, which are typical for the range explored in our investigations, we get $N \sim 10^{11}$.

Also the question may be raised whether the diffusive excitation process, that is made possible by the delocalization phenomenon, should not be significantly reduced by the spontaneous decay. However, the rate Γ_s of the latter process is much less than the diffusion rate Γ_D. Indeed even for orbital quantum number $l \sim 1$ the rate $\Gamma_s \sim (c^3 n_0^3 l^2)^{-1} \leq c^{-3} n_0^{-3}$ [34]. Estimating Γ_D by the inverse of the classical ionization time, i.e., by $\tau_I^{-1}\omega/2\pi$, with τ_I given by (6), we obtain:

$$\Gamma_s/\Gamma_D \sim 3\omega_0^{4/3}/(c^3\varepsilon_0^2) \sim 10^{-3}$$

* Actually a more refined analysis shows that in the two-dimensional case here considered one has localization on an exponentially large scale (see ref. [45] and eq. (4.4) of ref. [6]), so that delocalization takes place only slightly above (16).

where the numerical estimate is given for the typical values $\omega_0 = 1$, $\varepsilon_0 = 0.05$; notice also that the ratio does not depend on n_0. Actually, this ratio is even smaller because the extended state contains l up to $\sim\sqrt{n_0} \gg 1$.

2.3. *Ionization in the presence of localization*

According to the theory developed in the previous section, as long as the one-dimensional approximation is valid, the dependence of ionization on the field strength should have a more or less marked threshold character, defined by the quantum delocalization border (15). However, a microcanonical distribution of initial states looks fairly typical in many physical situations, so that it is interesting to investigate what should be in that case the dependence of ionization probability on the field intensity. Indeed, since the two-dimensional localization border (16) depends on both quantum numbers n_1, n_2, in that case we should expect that for any (not too "high") field, a fraction of the states, depending on the field strength, will be delocalized, while others will be localized and will therefore give no contribution to the ionization rate.

We will derive this dependence, under the assumption that the interaction time τ_{int} of the atom with the field is large enough for the classical system to undergo complete ionization, i.e., that the classical ionization probability $P_{\text{I}}^{\text{cl}} = 1$. Besides that, however, τ_{int} must not be so large that multiphoton quantum ionization from the stationary distribution (10) into the continuous spectrum becomes effective (see the comments in section 2.2).

Let's first assume that we have initially a homogeneous distribution of states with a fixed value of n_0 and of the magnetic quantum number m. Then, after the time τ_{int}, all atoms initially in states with $\varepsilon_0 > \varepsilon_{\text{q}}^{(2)}(n_2, m)$ will be ionized. These are precisely the atoms initially in states with $n_2 > n_2^{\text{cr}}$ given by the equation $\varepsilon_0 = \varepsilon_{\text{q}}^{(2)}(n_2^{\text{cr}}, m)$. Then, recalling that $n_1 + n_2 = n_0 - |m|$, we see that the fraction of atoms in the ensemble which will *not* be ionized at time τ_{int} is equal to $2n_2^{\text{cr}}/(n_0 - |m|)$ (the factor 2 is due to symmetry for exchanges $n_1 \leftrightarrows n_2$). Computing n_2^{cr} from eq. (16), we get:

$$n_2^{\text{cr}} = [(m^2 + n_0^2 A^2)^{1/2} - |m|]/2 \,. \tag{17}$$

The ionization probability is therefore given by:

$$P_{\text{I}} = 1 - 2n_2^{\text{cr}}/(n_0 - |m|) = 1 - \{[m^2 + n_0^2 A^2]^{1/2} - |m|\}/(n_0 - |m|)$$

where

$$A = 2\beta^2 \omega_0^{7/3} \varepsilon_0^{-2} n_0^{-2} \,. \tag{18}$$

Now let's assume that the initial distribution is microcanonical, i.e., that all quantum states with a fixed n_0 are equally represented in it. The full number of such states is n_0^2. For any given value of m, the number of non-ionized states at time τ_{int} for the given ε_0 is just $n_2^{\text{cr}}(m, \varepsilon_0)$. We must then sum over the different values of m; in doing this, however, we must remember that there is a classical value m_{cr} above which there is no ionization (9). Replacing the sum by an integral, we find that the fraction of non-ionized atoms at time τ_{int} for the given ε_0 is given by:

$$1 - P_I \approx (4/n_0^2) \int_0^{m_{cr}} n_2^{cr}(m, \varepsilon_0)\, dm\,.$$

The factor 4 in the above formula is due to symmetry with respect to exchanges $m \rightleftarrows -m$, $n_1 \rightleftarrows n_2$. The latter symmetry must be taken into account also in inserting the appropriate expression for n_2^{cr} in the integrand. Indeed, n_2^{cr} cannot exceed $(n_0 - |m|)/2$; otherwise, since the argument is symmetric in n_1, n_2, a supercritical value of n_2 would enforce a subcritical value of $n_1 = n_0 - |m| - n_2$. Therefore, n^{cr} in the above integral is actually the infimum between (17) and $(n_0 - |m|)/2$, i.e., it is given by (17) for $|m| < m_1 = n_0(1 - A^2)^{1/2}$, while, for $m > m_1$ it is equal to $(n_0 - |m|)/2$.

Then, assuming $m_{cr} \approx n_0$ (which, as we have already remarked, is legitimate for $\omega_0 \approx 1$), and evaluating the integral, we finally get the dependence of P_I on the field ε_0 in the following form:

$$P_I = (1 - A^2)^{1/2} - A^2 \ln\{[1 + (1 - A^2)^{1/2}]/A^2\} \tag{19}$$

where A is given by eq. (18).

Unfortunately, it would not be correct to use available experimental data as a check of (19), for the following reasons.

In the first place, whereas experimental data concern the frequency region $\omega_0 < 1$, the above described theory of localization was derived in the frequency region $\omega_0 > 1$, where 1st order resonances exist (the peculiarities of the excitation process for $\omega_0 < 1$ will be discussed in section 3.2).

Second, according to numerical data [16], in experiments the condition $P_I^{cl} = 1$ was not fulfilled after time τ_{int}; indeed, by increasing τ_{int} a further increase of P_I^{cl} was gotten. This fact makes impossible the comparison of available experimental data with (19).

Finally, we remind that the above relations were derived under the assumption of independent diffusion in both degrees of freedom, which is currently under study.

2.4. Comparison of diffusive and one-photon ionization

In the delocalization region $\varepsilon_0 > \varepsilon_q$ the quantum mechanism of suppression of classical diffusion is not at work and therefore one expects that the quantum electron will diffuse and ionize like the classical one. This fact has been numerically checked and will be discussed in section 3. The resulting diffusive excitation can hardly be described within the framework of conventional multiphoton theory; moreover, it usually takes place in a very different range of frequencies than considered there. In order to appreciate the effectiveness of this new ionization process, it is interesting to compare it with the familiar one-photon process.

To obtain a quantitative estimate for one-photon ionization, we shall first observe that any normalized energy eigenfunction for the unperturbed one-dimensional hydrogen atom (i.e. for the Hamiltonian (2) with $\varepsilon = 0$) can be written as $u(z) = z\,R(z)$, where $R(z)$ is a radial eigenfunction for the three-dimensional atom with orbital quantum number $l = 0$. Therefore, the matrix element for the photoelectric transition from the nth unperturbed level of the one-dimensional model (2) to the continuum state having energy $p^2/2 = -1/2n^2 + \omega$ is given by

$$R_{n,0}^{p,0} = \int dz\, z^3\, R_{n0}(z)\, R_{p0}(z) \tag{20}$$

where R_{n0}, R_{p0} are radial eigenfunctions for the three-dimensional atom with orbital quantum number $l=0$. (We assume R_{p0} to be normalized on the energy scale.)

For highly excited states $n \gg 1$ the integral (20) can be evaluated by semiclassical methods. In ref. [34] the following semiclassical value of dipole matrix elements for transitions from states (n, l) to $(p, l \pm 1)$ was found for $l \ll n$, $p \ll 1$ (notice the difference in normalization between (20) and ref. [34]):

$$R_{n,1}^{p,l\pm1} \approx -\mathrm{i}l^2[K_{2/3}(\omega l^3/3) \pm K_{1/3}(\omega l^3/3)]/(3^{1/2}\pi\omega n^{3/2})$$

where $K_\nu(\xi)$ are MacDonald functions. Considering that the 2nd term in square brackets is negligible for small l, and that for $\xi \to 0$, $K_{2/3}(\xi) \approx 0.459(3\pi)^{1/2}(3\xi/2)^{-2/3}$, we find the following semiclassical value for (20):

$$R_{n,0}^{p,0} \approx R_{n,0}^{p,1} \approx 0.459 \times 2^{2/3}(-\mathrm{i})n^{-3/2}\omega^{-5/3}/\sqrt{\pi}\,.$$

Then the transition probability per unit time is:

$$\Gamma_\Phi = (\pi/2)\varepsilon^2|R_{n,0}^{p,0}|^2 \approx 0.265\varepsilon^2/(\omega^{10/3}n_0^3) \tag{21}$$

and the ionization probability in one period of the external field is

$$Y_\Phi = (2\pi/\omega)\Gamma_\Phi \approx 1.67\varepsilon_0^2 n_0^2/\omega_0^{13/3} \tag{22}$$

(for $\omega_0 \geq n_0/2$). This value is 3/2 times larger than in ref. [34] due to averaging over the solid angle.

In order to compare the 1-photon ionization and the diffusive ionization we shall choose the optimal regime of each process. Then for 1-photon ionization we take $\omega \approx (2n_0^2)^{-1}$, so that $Y_\Phi \approx 34\varepsilon_0^2 n_0^{-7/3}$. Instead, for diffusive ionization we take $\omega \approx n_0^{-3}$ ($\omega_0 \approx 1$), and we estimate the ionization probability per period as $Y_D \approx \tau_I^{-1}$ with τ_I as in (6): $Y_D \sim 2\varepsilon_0^2$.

In this way we see that diffusive ionization, which takes place for a much lower frequency than 1-photon ionization, is a much more effective process than the latter:

$$Y_D/Y_\Phi \sim n_0^{7/3}/17\,. \tag{23}$$

In real physical time this ratio changes as each Γ is multiplied by its own optimal frequency which gives:

$$\Gamma_D/\Gamma_\Phi \sim n_0^{4/3}/8\,. \tag{24}$$

This ratio is still large for $n_0 \gg 1$.

A detailed analysis of the dependence of the ionization probability on frequency will be discussed in section 3.4.

2.5. *Ionization by tunneling and Keldysh parameter*

We shall now discuss some peculiarities of the excitation and ionization for quasi-classical states in the classically stable region $\varepsilon_0 < \varepsilon_{cr}$, $\omega_0 > 1$. In this case the classical motion from one resonance to the next one is forbidden by the presence of smooth invariant curves between them.

Due to this fact, excitation and ionization can take place either via a multiphoton transition or due to tunneling through the classically forbidden region. A distinction can then be made between the two opposite cases, when the perturbation is $\varepsilon z_{nn'} \ll 1/n^3$ small or large (see (15a)). In the former case, the most effective mechanism of excitation is the chain of one-photon transition with $1/2n^2 - 1/2n'^2 = \omega$ (see sec. 2.2) which leads to appearance of equidistant (in energy) peaks in the distribution f_n (see fig. 14a1). The ratio $\varepsilon z_{nn'} n^3 \sim \varepsilon\omega^{-5/3} \ll 1$ does not depend on n and therefore the perturbation theory holds for all chain of peaks. The probability of transition from one peak to the next one is small $\sim(\varepsilon\omega^{-5/3})^2$ and the ionization rate depends algebraically on ε_0:

$$\Gamma_I \sim (\varepsilon_0/\varepsilon_p)^{2k} n_0^{-3}; \qquad \varepsilon_p = \omega^{5/3} n_0^4 \tag{25}$$

where $k = n_0/2\omega_0$ is the number of photons required for the transition into continuum. In the opposite case when $\varepsilon_0 \gg \varepsilon_p$ but still $\varepsilon_0 < \varepsilon_{cr}$, tunneling becomes dominant, and we can reasonably expect Γ_I to depend on ε_0 according to

$$\Gamma_I \propto \tau_I^{-1} \exp[-cn_0(\varepsilon_{cr} - \varepsilon_0)/\varepsilon_0] \tag{26}$$

where c is a numerical constant of the order of unity, τ_I^{-1} represents the ionization rate from the chaotic component, and the exponential factor is assumed to describe tunneling into the classically forbidden region, on account of its analogy with the formula describing tunneling in a static field. The condition for applicability of (26) is

$$\varepsilon_p = \omega_0^{5/3}/n_0 \ll \varepsilon_0 < \varepsilon_{cr} \approx 1/(50\omega_0^{1/3}) . \tag{27}$$

In order that (27) holds, levels $n_0 \gg 50\omega_0^2$ are required, e.g., for $\omega_0 \approx 1$ levels with $n_0 \gg 50$ must be considered.

It is interesting to compare these results with Keldysh's theory for tunneling [35] in which an "adiabatic parameter" $Y = \omega/(\varepsilon n_0) = \omega_0/\varepsilon_0$ is introduced, discriminating the perturbative regime ($Y \gg 1$) from the tunneling regime ($Y \ll 1$). In the present case, (27) shows that in order that tunneling ionization according to (26) can take place it is necessary that $Y = \omega_0/\varepsilon_0 \gg 1$. For instance, for $\omega_0 \approx 1$, $\varepsilon_0 \approx 0.01$, $n_0 \gg 100$ eq. (27) is satisfied but $Y \approx 100$. Therefore, we see that here also, like in [35], the multiphoton regime occurs for weak field in the perturbative region ($\varepsilon_0 \ll \varepsilon_p$), whereas tunneling takes place in the opposite case of strong field ($\varepsilon_0 \gg \varepsilon_p$). So, the Keldysh parameter loses its usual meaning and a new parameter Y_H must be introduced in order to discriminate between the perturbative regime ($Y_H \gg 1$) and the tunneling regime ($Y_H \ll 1$). According to the previous discussion the new parameter Y_H will have the expression

$$Y_H = \omega_0^{5/3}/(n_0\varepsilon_0) = \omega^{5/3}/\varepsilon . \tag{28}$$

The reason of this deviation from the results of [35] is the presence of a large number of intermediate levels between the initial state and the continuum.

3. Numerical results

3.1. Methods of numerical simulation

In this section we shall describe the numerical methods and the checking procedures we used in our computer simulation of the classical and quantum dynamics of the one-dimensional model.

Reducing to one the dimension of the problem sharply decreases the computation time in the quantum case, and this allows for a more precise investigation of the excitation dynamics. The main computations were carried out on the CRAY-XMP Computer.

The numerical solution of the classical equations was carried out in action-angle variables (n, λ). As in [19], in order to circumvent the singularity at $z = 0$ a change was made to new variables (n, ξ) and to a new time η, which allow us to write the equations in the following form:

$$\begin{aligned} &\mathrm{d}n/\mathrm{d}\eta = -\varepsilon n^2 \cos \omega t \sin \xi \\ &\mathrm{d}\xi/\mathrm{d}t = n^{-3} + 2\varepsilon n \cos \omega t (1 - \cos \xi) \\ &\mathrm{d}t/\mathrm{d}\eta = 1 - \cos \xi ; \qquad \lambda = \xi - \sin \xi . \end{aligned} \tag{29}$$

A similar method for avoiding the singularity at the origin was used in [30]. Equations (29) were then numerically integrated by the Runge–Kutta method. The initial distribution of classical trajectories was taken on a line in phase space with $n = n_0$ and uniformly distributed phases λ; this choice corresponds to the initial condition used in the quantum case (only one level excited with $n = n_0$). The full number of classical trajectories was taken 250 or 1000.

An absorption mechanism was introduced for trajectories being excited above $n \approx 4n_0$. A change in the border of absorption only weakly affected the excitation probability.

The investigation of quantum dynamics described by the Hamiltonian (2) was carried out by two distinct methods. In the first one, following [19], a base of discrete unperturbed eigenstates was used, and the equations were solved for the amplitudes c_n of the expansion of the state vector over these eigenstates:

$$\mathrm{i}\dot{c}_n = -(1/2n^2)c_n + \varepsilon(t) \sum_{n'=n_{\min}}^{n_{\max}} z_{nn'} c_{n'} . \tag{30}$$

The value of $n_{\min}$ was approximately 20–40 levels lower than the initially excited state n_0. A further decrease of $n_{\min}$ did not appreciably influence the dynamics, owing to the exponential decrease of the distribution $f_n = |c_n|^2$ in the region $n < n_0$ where the classical motion is stable. A typical value for the full number of levels for which eqs. (30) were solved was $ND = n_{\max} - n_{\min} = 192$.

In order to numerically integrate (30) the time dependence of the field was approximated by $\varepsilon(t) = \Delta t\, \varepsilon \cos \omega t \, \Sigma_k \, \delta(t - k\,\Delta t)$ with $\Delta t = 2\pi/\omega L$, where L is the number of integration steps per period. This scheme of integration is physically equivalent to introducing supplementary fields with frequencies $\omega_k = kL\omega$, $k = 1, 2, \ldots$. Since in our computations $\omega \sim 1/n_0^3$ and the number L of steps was chosen between 100 and 500, then even the frequency $\omega_1 \approx 100\omega$ was much larger than all frequencies for transitions between intermediate levels. Therefore, the influence of the fictitious frequencies ω_k can be considered to be small.

The integration of the numerical scheme thus obtained can be carried out exactly; indeed, it reduces to successive applications of a matrix to a vector $c(t)$:

$$c(t+\Delta t) = \boldsymbol{T} \exp[-i\varepsilon_0(\cos \omega t_k)\,\Delta t\, z]\, c(t)$$
$$= \boldsymbol{TQZQ}^{-1} c(t)$$

where $\boldsymbol{T}$ and $\boldsymbol{Z}$ are unitary diagonal matrices, with $T_{n,n} = \exp(i\,\Delta t/(2n^2))$ and $Z_{n,n} = \exp[-i\varepsilon_0(\cos \omega t_k)\,\Delta t\, z_n]$, z_n are the eigenvalues of the matrix $z_{n,m}$, and $\boldsymbol{Q}$ is a unitary matrix that transforms the matrix $Z_{n,m}$ into diagonal form. With this procedure, the normalization $W = \Sigma_{n_{\min}}^{n_{\max}} |c_n|^2 = 1$ is conserved to a very high accuracy ($\sim 10^{-7}$). In [19, 22] the operator $\exp(-i\,\Delta t\, \varepsilon_0 z \cos \omega t_k)$ was computed, by means of its expansion in powers of Δt (up to the 5th order), which led to an effective damping on higher levels and to a poorer conservation of normalization. The new method used here appears significantly more efficient in that it permits to decrease the number of steps per period.

The main inconvenience with the just described integration scheme is that the continuous spectrum is completely neglected. Even though a number of arguments can be put forth [19, 22], suggesting that the continuous spectrum would not essentially modify the dynamics of excitation over discrete levels, nevertheless it is important to build a numerical model free of this shortcoming.

As far as we know, no numerical experiments were up to now performed, giving a precise account for continuous spectrum [52]. A partial consideration of transitions into the continuum, has been given in ref. [37]. However no account was there taken for continuum–continuum transitions, which, generally speaking, do not appear negligible as compared with transitions to and from the continuum. Moreover, the number of equations to be solved sharply increases with the level number n_0 and this does not allow for investigation of excited states with $n_0 \approx 60$.

A more efficient account for continuum can be given by means of the so-called Sturm basis. This basis is introduced by considering the following eigenvalue equation:

$$-\tfrac{1}{2}\, d^2u/dz^2 - (\beta/z)u = Eu\,, \qquad z>0,\ E<0,\ \beta>0\,. \tag{31}$$

For $\beta = 1$, (31) is just the Schrödinger equation for the stationary states of the unperturbed one-dimensional hydrogen atom. By changing variables according to $\xi = 2z$, $u(z) = (\xi/2)^{1/2} v(\xi)$, eq. (31) becomes

$$S_E v \equiv d/d\xi(\xi\, dv/d\xi) + [(E/2)\xi - 1/(4\xi)]v = -\beta v\,. \tag{32}$$

The Sturm basis is generated, by considering (32) as defining eigenvalues $-\beta$ for the operator S_E, where $E<0$ is an arbitrary fixed parameter.

Instead, considering in (32) β as parameter and E as the eigenvalues, one would recover to the usual basis, including continuum eigenfunctions.

It is known [29] that S_E is a self-adjoint operator with a purely discrete spectrum $\beta_s = (s+1)(-2E)^{1/2}$, with $s \geq 0$ an integer. Eigenfunctions for S_E are given by

$$f_s(\xi) = [(s+1)(-2E)^{1/2}]^{1/2}\, F(-s, 2, \xi(-2E)^{1/2})\, [\xi(-2E)^{1/2}]^{1/2}\, \exp[-(\xi/2)(-2E)^{1/2}]$$

and are orthonormal:

$$\int_0^\infty \mathrm{d}\xi\, f_s(\xi)\, f_{s'}(\xi) = \delta_{ss'} .$$

Here, and below, F with three variables will indicate the confluent hypergeometric function. In the following, we shall choose $E = -1/2n_0^2$, n_0 being the initially excited level. Then, $z^{1/2} f_{n_0-1}(2z)$ is, apart from a normalization constant, the n_0th unperturbed eigenfunction.

We also need matrix elements for ξ and ξ^2. For ξ^2 they are given in [29], where they are used in order to calculate the 2nd-order Stark effect. Matrix elements for ξ can be obtained by direct computation.

Non-zero elements for ξ and ξ^2 are then given by:

$$\begin{aligned}
&\xi_{s,s} = 2n_0(s+1) \\
&\xi_{s-1,s} = \xi_{s,s-1} = -n_0[s(s+1)]^{1/2} \\
&(\xi^2)_{s,s} = 6n_0^2(s+1)^2 \\
&(\xi^2)_{s,s-1} = (\xi^2)_{s-1,s} = -2n_0^2(2s+1)[s(s+1)]^{1/2} \\
&(\xi^2)_{s,s-2} = (\xi^2)_{s-2,s} = n_0^2 s(s^2-1)^{1/2} .
\end{aligned} \tag{33}$$

Let now $\phi(t) = z^{1/2}\psi(t)$ be the solution of the Schrödinger equation with the Hamiltonian (2), and $z = \xi/2$. Then, $\frac{1}{4}\int_0^\infty \xi|\psi|^2\,\mathrm{d}\xi = 1$. Since the f_s's make up a complete orthonormal set, ψ can be expanded in the form

$$\psi(t) = \sum_{s=0}^{\infty} A_s(t) \exp(-\mathrm{i}E_0 t)\, f_s$$

with $E_0 = -1/2n_0^2$ and $\psi(0) = (2^{1/2}/n_0)\, f_{n_0-1}$ corresponding to the initially excited level n_0. By using the orthonormality of the f_s and the expression (33) for matrix elements, from the Schrödinger equation we obtain equations for the amplitudes $A_s(t)$:

$$\begin{aligned}
&2(s+1)\dot{A}_s - [s(s+1)]^{1/2}\dot{A}_{s-1} - [(s+1)(s+2)]^{1/2}\dot{A}_{s+1} \\
&\quad = -\mathrm{i}\{[2(s+1-n_0)/n_0^2]A_s + 3\varepsilon(t)\, n_0(s+1)^2\, A_s - \varepsilon(t)\, n_0[(2s+1)\,(s(s+1))^{1/2}\, A_{s-1} \\
&\qquad + (2s+3)\,((s+1)(s+2))^{1/2}\, A_{s+1}] + (n_0/2)\,\varepsilon(t)\,[s(s^2-1)^{1/2}\, A_{s-2} \\
&\qquad + (s+2)((s+2)^2-1)^{1/2}\, A_{s+2}]\} .
\end{aligned} \tag{34}$$

This infinite system of equations is exact and, even though only a discrete base was used, it completely takes into account the continuum. Indeed, each Sturm function is a superposition of several eigenfunctions from the unperturbed base, including eigenfunctions belonging to the continuous spectrum.

Once eqs. (34) have been solved for A_s, the original amplitudes $c_n(t)$ of the expansion of $\phi(t)$ over the unperturbed eigenstates

$$u_n(z) = 2zn^{-3/2}\, e^{-z/n} F(-n+1, 2, 2z/n)$$

can be recovered by

$$c_n(t) = \sum_s B_{ns}\, A_s(t)$$

where the transformation matrix B_{ns} from the Sturm to the unperturbed base is given by

$$\begin{aligned} B_{ns} &= \tfrac{1}{2} \int_0^\infty d\xi\, (\xi/2)^{1/2}\, f_s(\xi)\, u_n(\xi/2) \\ &= 4(s+1-n_0)\,[2(s+1)n]^{1/2}\,(n_0-n)^{s+n-2}\,(n_0 n)^2\,(-1)^n\,[(n_0+n)^{s+n+2}]^{-1} \\ &\quad \times F(-s, -(n-1), 2, -4n_0 n/(n-n_0)^2)\,. \end{aligned}$$

Here F is Gauss' hypergeometric function. A similar computation, for continuous spectrum unperturbed eigenfunctions can be made, by simply substituting i/p in place of n, p being the electron momentum (an analogous method was used, e.g., in [34]). A method for computing F with large s, n is given in appendix IV.

The numerical integration of eqs. (34) was performed as follows. One level $s_0 = n_0 - 1$ was initially excited, so that $A_s(0) = (2^{1/2}/n_0)\,\delta_{s,n_0-1}$. Then eqs. (34) were solved for $s_{\min} \le s \le s_{\max}$. As a rule, $s_{\min} \approx 10$–30, and the full number NS of Sturm levels ranged from 256 to 576. The dependence of the field on time was taken in the same way as in the previously decribed method, with approximately the same number of steps per period: $100 < L < 500$. Just as in the 1st method, the introduction of delta functions into the numerical scheme made it possible to exactly integrate the truncated set of equations (34) by repeated applications of matrices. For the same reason, the loss of normalization was very small ($\sim 10^{-7}$). Unlike the 1st method, here the presence of high frequencies $\omega_k = kL\omega$ led to direct transitions into the continuum; however, for the chosen values of L the probability of such transitions was negligibly small. For instance, for $n_0 = 60$, $\omega_0 = 1$, $\varepsilon_0 = 0.1$, $L = 100$ we get $\omega_1 n_0^3 = 100$ and the ratio of one-photon ionization (21) to the diffusive one (6) is of the order 5×10^{-4}. Therefore the small δ-function kicks introduced by the numerical simulation of the monochromatic perturbation do not have any effect on the physics of the problem; moreover, their influence can be kept under control by varying the integration step.

In our opinion, monochromaticity of the perturbation is important for this problem, and substituting a δ-like perturbation $\Sigma_k\, \delta(t - 2\pi k/\omega)$ in place of $\varepsilon \cos \omega t$ [38, 39] can lead to a significant modification of the physical picture of multiphotonic excitation. The role of multiphoton transition in the two-dimensional model with a δ-like perturbation was studied in ref. [38].

The values of $A_s(\tau)$ obtained by integrating (34) were used to find the amplitudes $c_n(\tau)$ over the unperturbed discrete base by means of the transformation matrix B_{ns}. In this way $c_n(\tau)$ were found for approximately 200 levels. Since the total probability was conserved with high accuracy, it was then possible to determine the probability of excitation above a given level, and also the probability of transition into the continuum, which is included in the former.

Several characteristics of the excitation were computed by the described numerical method. Among them, the most important were the distribution over unperturbed levels $f_n = |c_n|^2$, the 1st moment $M_1 = (\langle n \rangle - n_0)/n_0$, the 2nd moment $M_2 = \langle (\Delta n)^2 \rangle = \langle (n - \langle n \rangle)^2 \rangle / n_0^2$, and the probability of excitation to high levels. In order to describe the latter we considered the probability $W_{1.5}$ of excitation to states with $n \geq [1.5 n_0]$, where [ ] means the integral part. For computations in Sturm base, this probability included also the probability of ionization, namely $W_{1.5}$ is the total probability in states $n \geq 1.5 n_0$ plus the probability in the continuous part of the spectrum. In order to eliminate fluctuations, we also determined the distribution f_n averaged over $\Delta\tau$ periods of the field; as a rule, $\Delta\tau$ was chosen 40 or 60. Finally, we determined the average distance of the electron from the nucleus, $\langle z \rangle$.

The accuracy of the numerical results was checked as follows. First, in order to check that continuous spectrum was being properly taken into account, we performed a series of experiments with frequencies larger than the 1-photon ionization threshold, $\omega_0 > n_0/2$. In the absence of resonances within the discrete spectrum, the probability on discrete levels with $n \geq 1.5 n_0$ was then negligibly small, so that the probability of ionization $W_I \approx W_{1.5}$. An example of dependence of W_I on time is shown in fig. 1. In fig. 2 we show a comparison of the theoretical ionization rate with the numerically obtained one. As can be seen, there is an excellent agreement with the theory of 1-photon ionization (22), which indicates that computations in the Sturm basis efficiently reproduce continuum effects.

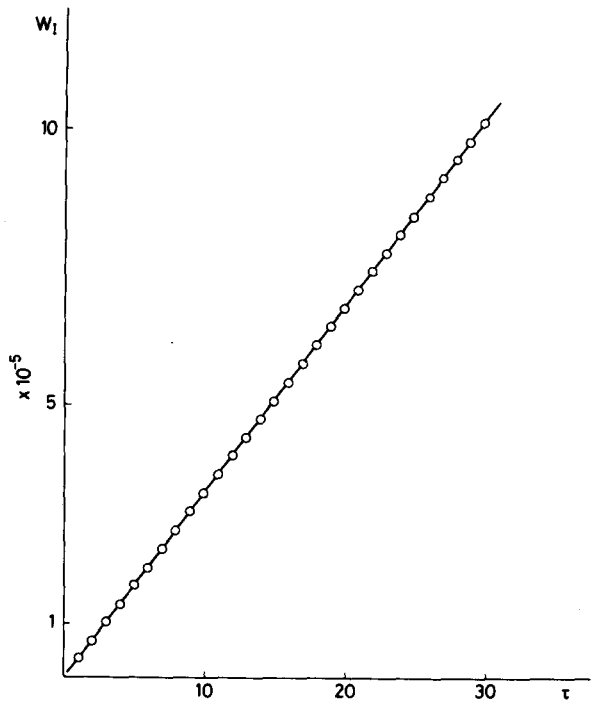

Fig. 1. Ionization probability W_I as a function of time τ (number of microwave periods) for the case $n_0 = 30$, $\omega_0 = 30$, $\varepsilon_0 = 0.075$. The solid line is drawn according to the analytical expression (22) while the circles are the results of our quantum numerical computations. The excellent agreement with the theory even for very large frequencies is a check of our numerical computations and shows that the Sturm basis efficiently takes into account the continuous spectrum.

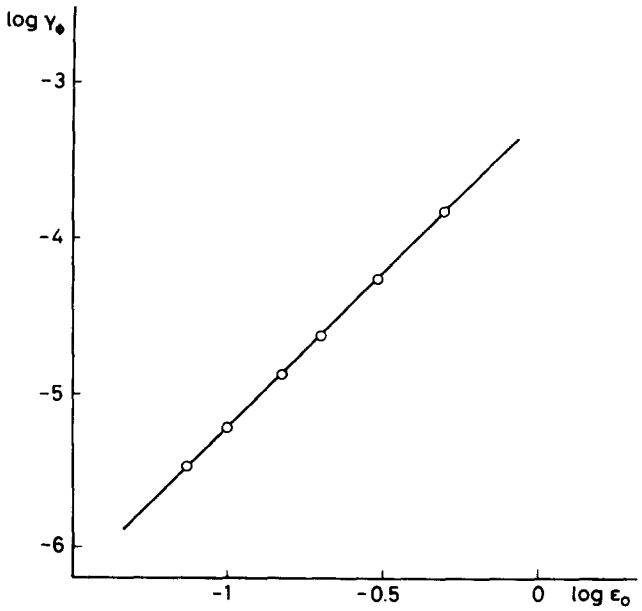

Fig. 2. Ionization rate versus field strength for the case $n_0 = 30$, $\omega_0 = 30$. Like in fig. 1, the straight line is drawn according to the theoretical expression (22) and the circles are results of quantum numerical computations. Here also notice the very good agreement between theory and numerical results.

A different type of check was gotten by increasing the number L of integration steps per period. The relative changes of the characteristics of excitation produced in this way were very small. For instance, in the 1st method (unperturbed base, UB) with $n_0 = 66$, $\omega_0 = 1.5$, $\varepsilon_0 = 0.04$, a change of L from 200 to 300 for $\tau = 120$ led to a relative change $\Delta W_{1.5}/W_{1.5} \approx 10^{-3}$, $\Delta\langle z\rangle/\langle z\rangle \approx 5 \times 10^{-4}$. Of the same orders were also the changes in the Sturm basis (SB), even for rather small values of $W_{1.5}$. For instance, for $n_0 = 66$, $\omega = 2$, $\varepsilon_0 = 0.03$, $\tau = 120$, $W_{1.5} \approx 4 \times 10^{-4}$, upon changing L from 100 to 200 the relative change in probability and in $\langle z\rangle$ were $\Delta\langle z\rangle/\langle z\rangle \approx \Delta W_{1.5}/W_{1.5} \approx 5 \times 10^{-3}$. We can therefore assume that for sufficiently large L the effects of numerical discretization in the integration of (30) and (34) become negligibly small, and have no influence on the physics of the problem.

A further check consisted in changing the total number of levels both in the Sturm and in the unperturbed base, and also in matching the excitation characteristics obtained by the two different methods. One such comparison is shown in fig. 3a, where it can be seen that there is a good agreement between results of computations in UB and in SB, and also that an increase in the number of Sturm levels does not change significantly the excitation probability (which includes continuum). Such an agreement not only takes place for integrated characteristics, but also for the distribution over unperturbed levels (fig. 4). It is then possible to conclude that continuum effects do not lead to substantial modifications of the excitation dynamics, at least for not too strong fields and high frequencies. Moreover, the Sturm basis used in our computations appears large enough to provide a satisfactory model for quantum dynamics, including continuum.

Finally, the agreement we found between classical and quantum computations in the delocalization regime, as we shall discuss in the next section, provides, in our opinion, the most convincing element in support of our methods.

We also checked that the localization of the extended states in a more realistic two-dimensional

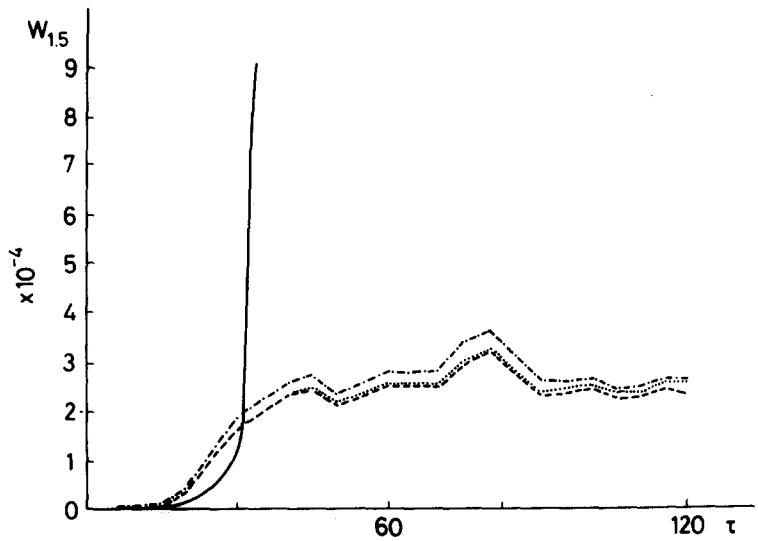

Fig. 3a. Excitation probability $W_{1.5}$ as a function of time τ for the case $n_0 = 66$, $\varepsilon_0 = 0.04$, $\omega_0 = 2.5$. The quantum numerical computations are performed by using: i) the unperturbed base with $ND = 192$ eigenstates (– · –); ii) the Sturm basis with $NS = 384$ (· · · ·); iii) the Sturm basis with $NS = 576$ (– – –). The fairly good agreement of the three curves is a check of the numerical computations. The classical ionization curve is also shown (solid line).

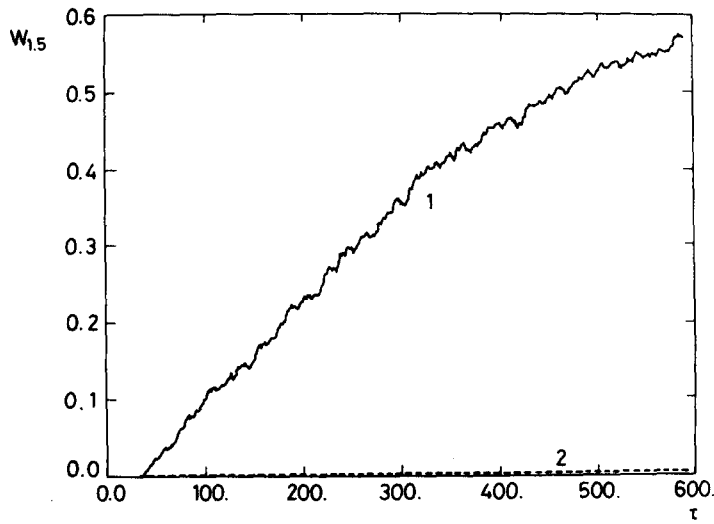

Fig. 3b. Classical (1) and quantum (2) excitation probability $W_{1,5}$ as a function of time for the same case as in fig. 3a.

model is very close to that in our one-dimensional model as shown in fig. 7c. This is in no contradiction with recent results [53] on the instability of classical extended orbits in the resonant electric field ($\omega_0 = 1$). First, we mainly use nonresonant fields (e.g. fig. 7c). Second in the chaotic component of the motion even for $\omega_0 = 1$ only a slow diffusion in n_2 takes place according to eq. (7).

The dynamics of quantum excitation was investigated for $n_0 = 30, 45, 66, 100$, and the field ranged in the interval $0.01 < \varepsilon_0 < 0.34$. In order to facilitate conversion to physical units, we note that for $n_0 = 100$

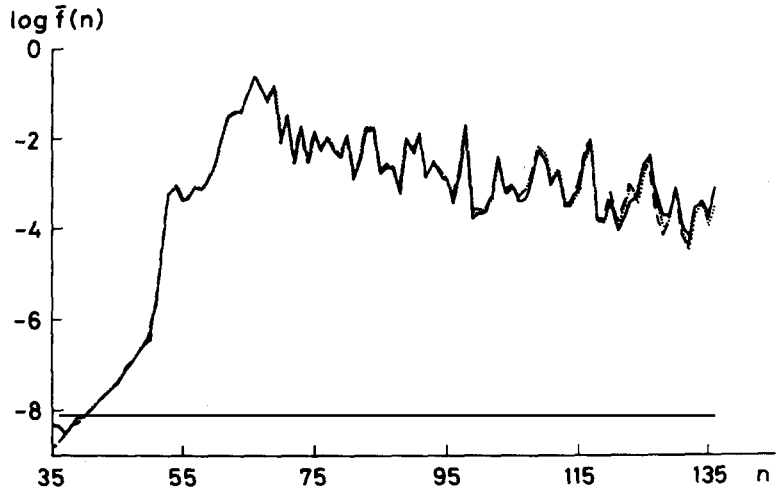

Fig. 4. Quantum probability distributions $\bar{f}(n)$ over the unperturbed states averaged over 60 values of $\tau = \omega t/2\pi$ within the interval $60 < \tau < 120$. Here $n_0 = 66$, $\varepsilon_0 = 0.04$, $\omega_0 = 1.5$. Three different curves are plotted in the Sturm basis with $NS = 384$ and $NS = 576$ and integration in the unperturbed basis with $ND = 192$. The three curves are so close that they are not resolved in the graph and this is an additional check on the accuracy of numerical computations.

the frequency $\omega/2\pi = 10\,\text{GHz}$ corresponds to $\omega_0 = \omega n_0^3 = 1.51998$, and $\varepsilon_0 = \varepsilon n_0^4 = 0.1$ corresponds to $\varepsilon = 5.14485\,\text{V/cm}$.

For clarity's sake we have grouped our numerical results following the order of the previous theoretical analysis. Therefore we shall now discuss, in turn, the results on the classical model, the results demonstrating the localization phenomenon, and the results illustrating the dependence of the excitation probability on the field frequency.

3.2. *Numerical results on the classical model*

The dependence of the excitation probability of the classical system on the frequency ω_0 and strength ε_0 of the field is shown in fig. 5. Here the excitation probability $W_{1.5}$ is computed after $\tau = 40\omega_0$ periods of the external field. We recall that the initial value n_0 is irrelevant due to the scaling property of the classical motion. The characteristic oscillations with minima near integer values of ω_0 are connected with the presence of nonlinear resonances, the strongest of which correspond to integer ω_0. In fact, the destruction of the centers of resonance regions occurs for larger fields than the critical field for resonance overlap, eq. (3).*

Then, for not too strong fields, only a fraction of the trajectories from the initial distribution, which is uniform in space, diffuse to higher values of n, but the rest fall into the central stable region of resonance, where they remain giving no contribution to $W_{1.5}$.

The characteristic dip for $\omega_0 = 0.5$, which was also observed in numerical experiments on two-dimensional atoms [41] corresponds to a 2nd order (half-integer) resonance. The sharp maximum of $W_{1.5}$ for $\omega_0 \approx 0.7$ (weakly depending on ε_0) is due to the fact that for this frequency most trajectories fall into the stochastic layer of the separatrix of the big fundamental resonance $\omega_0 = 1$. Already after half a turn around the resonance they pass into the high-n region, where excitation is significantly stronger.

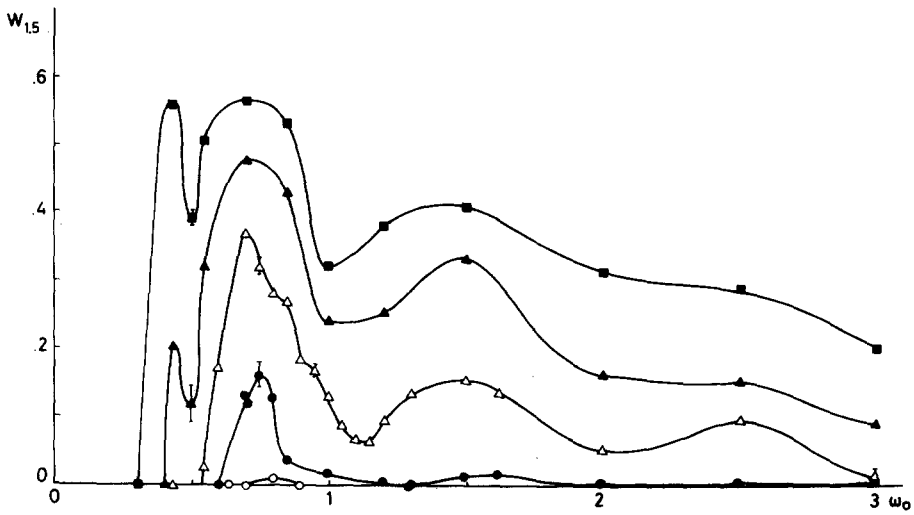

Fig. 5. Classical ionization probability $W_{1.5}$ after $\tau = 40\omega_0$ as a function of the microwave frequency for different microwave fields. Here $W_{1.5}$ is the total probability above the action value $n = 1.5n_0$. (○) $\varepsilon_0 = 0.02$; (●) $\varepsilon_0 = 0.03$; (△) $\varepsilon_0 = 0.04$; (▲) $\varepsilon_0 = 0.05$; (■) $\varepsilon_0 = 0.06$.

* The values of the field at which the centers of resonance regions are destroyed were numerically determined in [30].

An analogous excitation mechanism, connected with the 2nd order resonance at $\omega_0 = 0.5$, explains also the maximum at $\omega_0 = 0.43$.

In the classical system diffusive excitation takes place only when the field strength exceeds the critical value for which the last KAM invariant curve is destroyed and there is a transition to global stochasticity (see e.g., [5]). From fig. 5 we see that the actual value of ε_{cr} for $\omega_0 \approx 1$ is close to 0.02, which satisfactorily agrees with the theoretical value (3) obtained by the resonance overlap criterion [5]. Figure 5 gives an overall idea of the classical behavior. Other numerical results such as the comparison with the solution of the diffusion equation or with the quantum distribution on the unperturbed levels will be given in the following sections.

3.3. *The distribution over the unperturbed levels*

Here we shall describe the features of the numerically computed quantum distribution over the unperturbed levels in the various parameter regions which have been discussed in our previous theoretical analysis. In this way we shall show that numerical results support the theoretical estimates given above.

For high levels (e.g. $n_0 \approx 100$) and $\varepsilon_0 \approx \varepsilon_{cr} \approx 0.02$ the perturbation strength $V = \frac{3}{2} n^2 \varepsilon$ is larger than the level separation: $V/\Delta E \approx \frac{3}{2} \varepsilon_0 n > 1$, so that the field would be expected to connect a number of unperturbed levels. Yet, even for $\varepsilon_0 n \gg 1$ no diffusive excitation will be observed if $\varepsilon < \varepsilon_{cr}$. (The opposite case $\varepsilon_0 n \ll 1$ corresponds to the region below the "quantum stability border" [36].) This is illustrated in fig. 6, where an example of stationary distribution in the region of stability $\varepsilon < \varepsilon_{cr}$ is shown. This distribution remains essentially unchanged upon further increasing the computation time. Classically, this fact is due to the stability of the motion, and quantum mechanically to the very small probability of tunneling into regions classically forbidden by the smooth invariant curve (section 2.5). However, for a reliable detection of the tunneling described in section 2.5 particularly accurate investigations are required. It is also desirable to increase n_0, because even for $n_0 = 100$ the tunneling region appears rather narrow (see eq. (27)). Nevertheless, we think that tunneling excitation can be

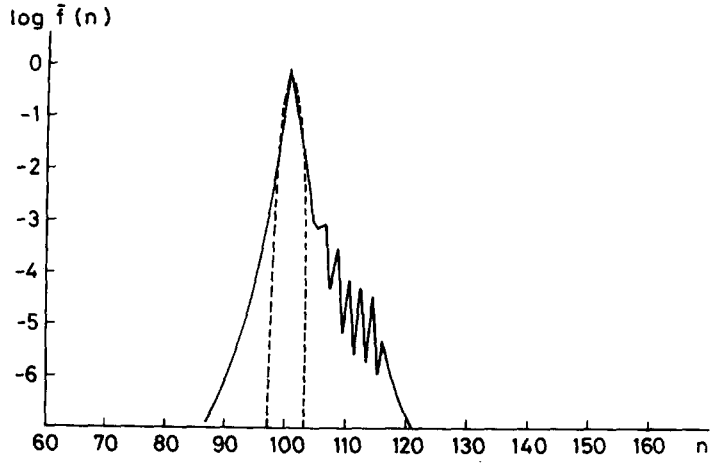

Fig. 6. Classical (dashed line) and quantum (full line) probability distribution $\bar{f}(n)$ averaged over 40 values of τ within the interval $80 < \tau < 120$. Here $n_0 = 100$, $\varepsilon_0 = 0.01$, $\omega_0 = 1.5$. For these parameter values, $\varepsilon_0 < \varepsilon_{cr} < \varepsilon_q$ and therefore both classical and quantum packets are localized. Notice the small tunneling through the classical KAM invariant curves.

investigated both in numerical and in laboratory experiments, where at the present time it is possible to prepare states with $n_0 \approx 300$ [26]. We also note, that clear experimental observations of tunneling excitation in alternating fields are still lacking.

For field strength exceeding the critical value (3), diffusive excitation takes place in the classical system. However, in the quantum case, for field strength less than the delocalization border (15) the phenomenon of quantum localization is observed, in consequence of which the distribution over the unperturbed levels reaches the stationary form (10) and then does not change upon increasing the time of interaction with the field. In this situation, the ionization probability is very small, and can be neglected for the given interaction time. A typical example of quantum localization is shown in fig. 7. Here we see that classically there is a diffusive excitation, so that the classical distribution obtained by the numerical simulation satisfactorily agrees with the theoretical formula (5a) (the classical border of stability was here chosen at $n^* = 55$ according to numerical results). The quantum distribution was obtained by the Sturm basis method with $NS = 576$; here, as well as in fig. 4, there is a good agreement with the results of computations by the unperturbed basis method. In contrast with the classical result, in the quantum case an exponential drop followed by a multiphoton plateau is observed, almost unchanged under a change of τ from 120 to 600. The quantum limitation of chaos also led to a significantly lesser excitation probability in the quantum than in the classical case (see also fig. 3). We mention here that in a recent paper [51] results of different quantum computations were reported with ionization probability 10% (to be compared to ours less than 7%) for $\omega_0 = 1$, $\varepsilon_0 = 0.03$, $n_0 = 63$ and $\tau = 320$ periods.

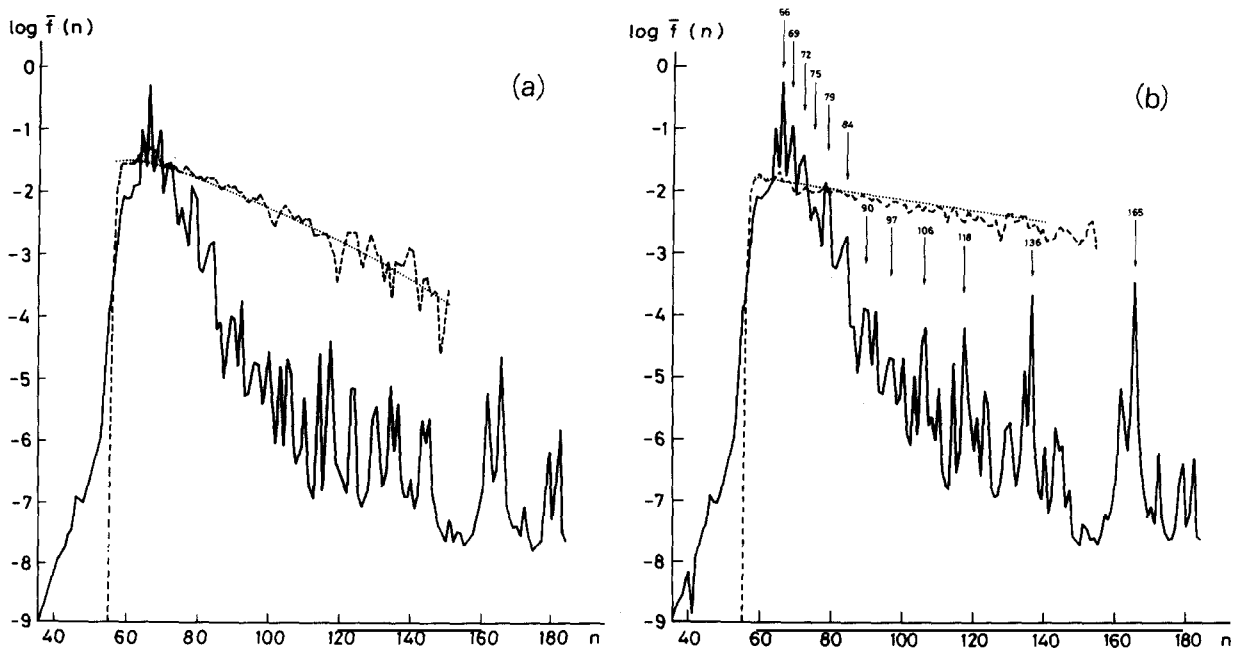

Fig. 7. Classical (dashed curve) and quantum (solid curve) probability distribution $\bar{f}(n)$ averaged over 40 periods of τ for the case $n_0 = 66$, $\omega_0 = 2.5$, $\varepsilon_0 = 0.04$. In (a) the average within the interval $80 < \tau < 120$ and in (b) within the interval $560 < \tau < 600$ are given. The dotted lines in both figures represent the analytical solution (5a) of the Fokker–Planck equation which fairly agrees with the classical numerical results. On the contrary, the quantum distribution is localized and does not change significantly by increasing the interaction time with the microwave from 120 to 600. The only difference between the quantum distributions is the slight increase of the peaks on the low multiphoton plateau. The arrows with integers show the position and the principal quantum numbers of the peaks.

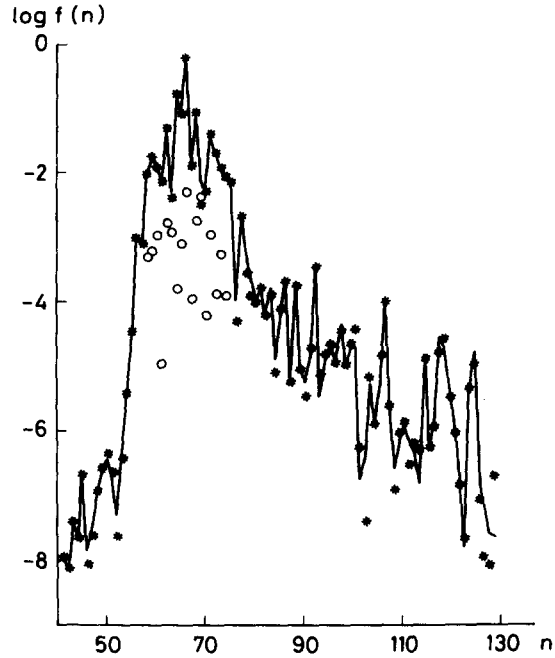

Fig. 7c. Comparison of one-dimensional (*) and two-dimensional (full curve) models for extended states; parameters as in fig. 7a,b and initial condition $n_2 = 0$(two-dimensional). Instant distributions f_n are given at $\tau = 60$. The circles show values of $\log|\Delta f_n|$ where Δf_n is the difference between the two models.

Another convincing manifestation of localization was the saturation of the diffusive growth of the second moment of the quantum distribution (fig. 8). The agreement between quantum and classical dynamics here holds only over a small initial time interval $\tau_D \approx 5$. The smallness of τ_D is due to the smallness of the classical diffusion rate. Notice that the agreement observed for $\tau < \tau_D$ provides still another check of the numerical procedure used.

In fig. 9 it is shown how the normalized average distance $RL = \langle z(t) \rangle / n_0^2$ of the electron from the

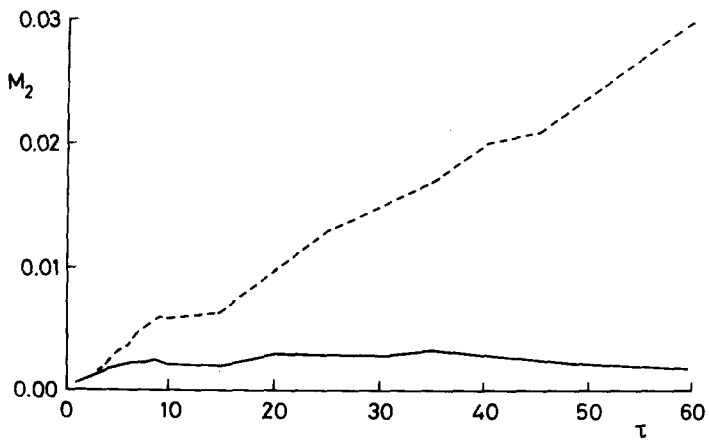

Fig. 8. Second moment $M_2 = \langle (n - \langle n \rangle)^2 \rangle / n_0^2$ of the classical (dashed line) and quantum (full line) distribution as function of time $\tau = \omega t / 2\pi$ for the parameters of fig. 7. The localization of the quantum packet shown in that figure leads here to the suppression of the diffusive growth of the moment M_2.

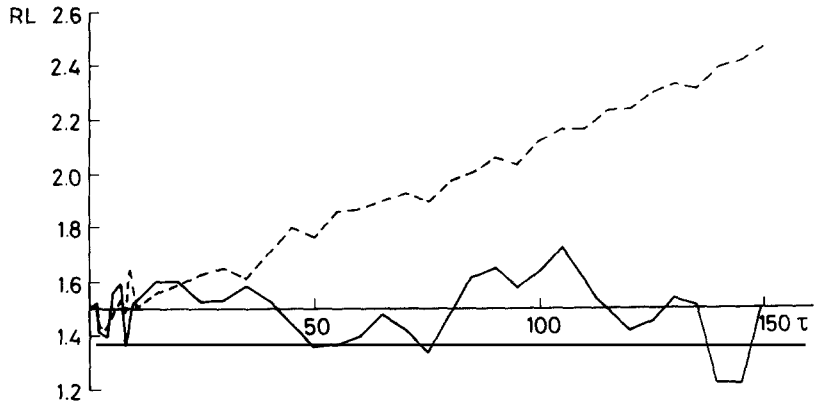

Fig. 9. Normalized average distance $RL = \langle z(\tau) \rangle / n_0^2$ of the electron from the nucleus as a function of τ for the same case as in fig. 7: (full line) quantum case; (dashed line) classical case. Also here the quantum suppression of diffusion is clearly manifested.

nucleus depends on time. In the classical system this distance grows and the electron moves far away from the nucleus. Instead, in the quantum case, owing to quantum localization, the electron keeps oscillating around its initial position.

The regime of quantum localization was investigated for initial levels $n_0 = 30$, 45, 66, 100, for frequencies $1 \leq \omega_0 \leq 3$, fields $0.03 \leq \varepsilon_0 \leq 0.12$, and localization length $l \gg 1$ (which is the condition for applicability of the estimate (11)). Numerical values for the localization length were determined directly from the stationary quantum distribution. Comparison of these numerical data with the theoretical values (eqs. (13), (14)) yields good agreement (fig. 10). The observed dispersion of points is apparently connected with the presence of islands of stability in the classical system. Also, the presence of a typically quantum resonance structure may play a role in this respect.

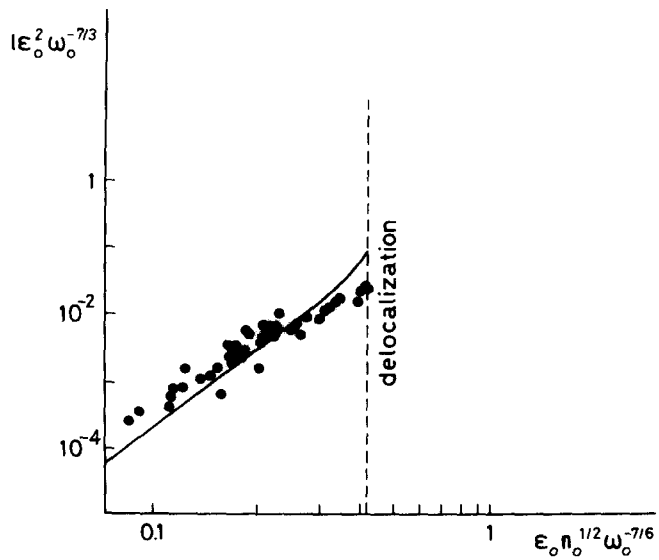

Fig. 10. Localization length as a function of the model parameters. The dots correspond to numerically measured values of l which are in good agreement with the solid curve given by the analytical estimate (13).

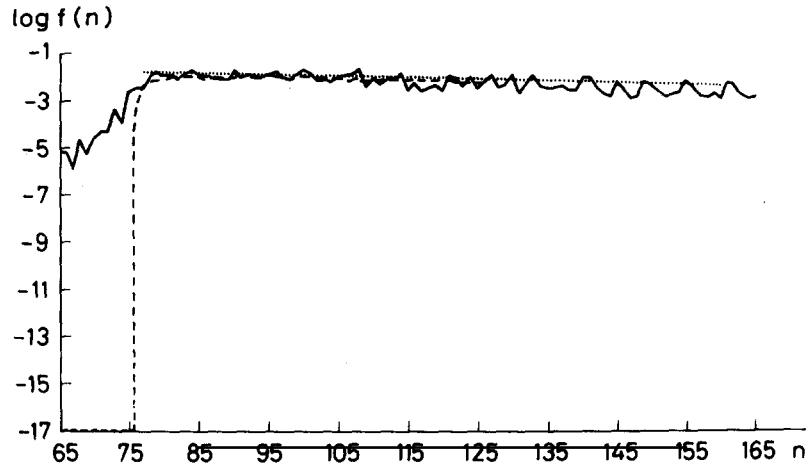

Fig. 11a. Classical (dashed curve) and quantum (full curve) distribution function $f(n)$ for $n_0 = 100$, $\varepsilon_0 = 0.08$, $\omega_0 = 1.5$ at $\tau = 60$. Notice the fairly good agreement between classical and quantum numerical results and the analytical solution given by eq. (5a) (dotted curve).

If the field exceeds the quantum delocalization border (15) then the quasi-classical diffusion over the levels is sufficiently fast and no localization takes place. In this regime the evolution of the distribution function can be approximately described by the diffusion equation (4). An example of a distribution in the delocalization regime is shown in fig. 11a, where it can be seen that the quantum distribution agrees with the solution (5a) of the Fokker–Planck equation.

In order to check the validity of the estimate (15) for the delocalization border, we investigated the dependence of the excitation probability on ε_0 for different values of n_0 and of ω_0. This dependence on the rescaled field $\tilde{\varepsilon}_0 = \varepsilon_0/\varepsilon_q^{(1)}$ is shown in fig. 13. For each value of n_0, ω_0, the excitation probability $W_{1.5}$

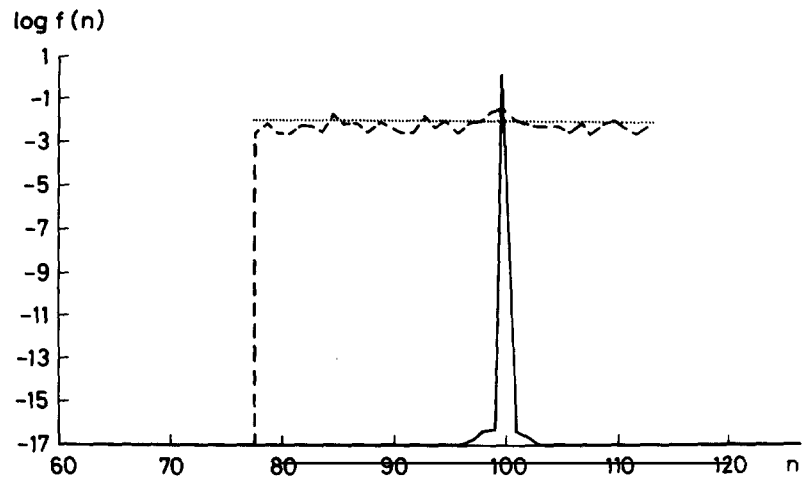

Fig. 11b. Probability distribution over the unperturbed states at $\tau = 120$ for the case of fig. 11a, after reversal of velocities at $\tau = 60$. Notice that the quantum system (full curve) recovers its initial state to seventeen digits which corresponds to numerical errors. In contrast, the classical motion (dashed curve) proceeds according to the diffusion equation (5a) (dotted curve).

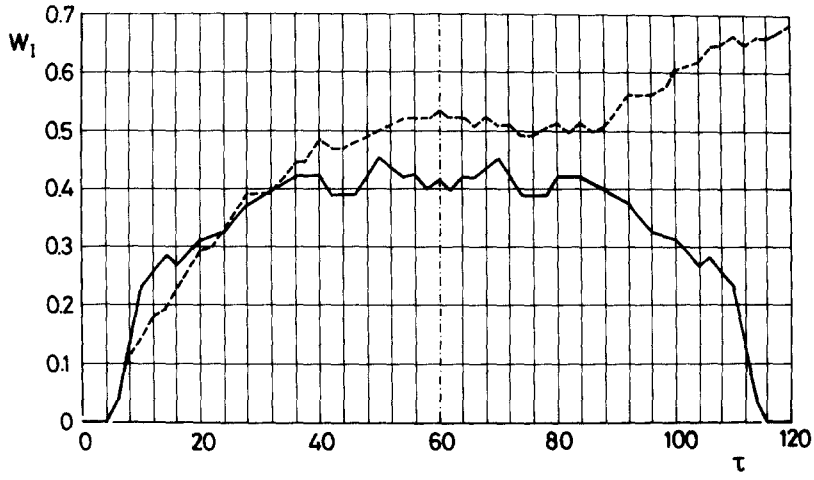

Fig. 12. Classical (dashed curve) and quantum (full curve) ionization probability (excitation above the unperturbed level $\bar{n} = 150$) as a function of time for the case of fig. 11. Notice the perfect specular symmetry of the quantum curve about the time of reversal $\tau = 60$.

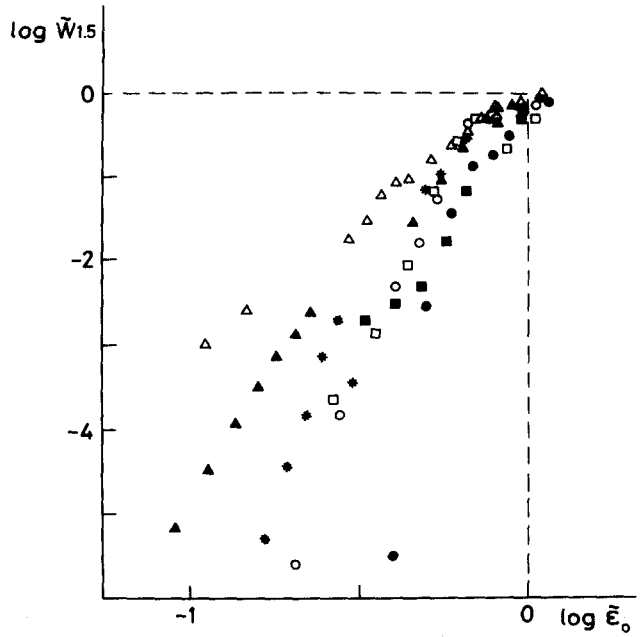

Fig. 13. Excitation probability at time $\tau = 60$ as a function of the field intensity for different values of n_0 and ω_0. $\tilde{W}_1(\tilde{\varepsilon}_0) = W_1^q(\varepsilon_0)/W_1^{cl}(\varepsilon_q^{(1)})$ is the quantum excitation probability at ε_0 rescaled to the corresponding classical excitation probability computed at $\varepsilon_0 = \varepsilon_q^{(1)}$; $\tilde{\varepsilon}_0 = \varepsilon_0/\varepsilon_q^{(1)}$ is the rescaled field: (△) $n_0 = 30$, $\omega_0 = 3$; (■) $n_0 = 45$, $\omega_0 = 1$; (▲) $n_0 = 45$, $\omega_0 = 3$; (●) $n_0 = 66$, $\omega_0 = 1$; (□) $n_0 = 66$, $\omega_0 = 2$; (*) $n_0 = 66$, $\omega_0 = 3$; (○) $n_0 = 100$, $\omega_0 = 3$. The fact that all points corresponding to different n_0 and ω_0 meet at the value $\tilde{W} = 1$ for $\tilde{\varepsilon}_0 = 1$ is a numerical verification of our estimate (15); it also verifies that, in the delocalized regime, the quantum excitation probability is close to the classical value.

was also rescaled to the corresponding classical value taken for $\varepsilon_0 = \varepsilon_q^{(1)}$; in other words, in fig. 13 we actually plotted $\tilde{W}_{1.5}(\tilde{\varepsilon}_0) = W_{1.5}^{q}(\varepsilon_0)/W_{1.5}^{cl}(\varepsilon_0)|_{\varepsilon_0=\varepsilon^{(1)}}$. If delocalization takes place for $\varepsilon_0 \approx \varepsilon_q^{(1)}$, and if in the delocalization regime the excitation probability keeps close to its classical value, then all the lines showing the dependence of $\tilde{W}_{1.5}(\tilde{\varepsilon}_0)$ for different values of n_0, ω_0 would be expected to meet for $\tilde{\varepsilon}_0 = 1$ at the value $\tilde{W}_{1.5} = 1$. As can be seen from fig. 13, this is just what happens.

An interesting feature of fig. 13 is that the dependence of the ionization probability on the field strength at fixed n_0 and ω_0 is not always monotonic. For example, the data corresponding to $n_0 = 66$, $\omega_0 = 3$ clearly indicate a "bump" occurring in the ionization curve. The existence of similar "bumps" in experimentally obtained ionization curves was recently pointed out in [48] and a theoretical explanation was put forth in [49].

In the localization regime, the dependence of the excitation probability on field can be approximately described by $\tilde{W}_{1.5} \propto \tilde{\varepsilon}_0^{2k}$. Figure 13 also clearly indicates that the experimental value of k changes substantially with n_0, ω_0, so that joining of all lines at a single point for $\tilde{\varepsilon}_0 = 1$ is not a trivial occurrence, and can be considered as a confirmation for our estimate (15). This diversity in the values of k is connected with the different number of photons which are required for excitation into states with $n \geq [1.5n_0]$. However, the experimentally determined value k_E is typically, substantially less than the number k_D of photons theoretically required for direct transition from n_0 to $n \approx 1.5n_0$, which is $k_D = 1 + [5n_0/18\omega_0]$. For example, for $n_0 = 66$ and $\omega_0 = 1$, one has $k_E \approx 7$, $k_D = 19$.

In our opinion this difference is due to two effects. The first is that multiphoton transitions do not necessarily start from the initial unperturbed state, but may start from anywhere inside the stationary distribution (10) which sets up after a while. In other words, when $l > 1$ excitation may start from levels $n \sim n_0 + l$, and this reduces the multiphotonic degree k. The other reason is the appearance, for high levels $n > n_0$, of a multiphoton plateau of equidistant resonances [22]. Examples of distributions $\bar{f}_n$ which clearly exhibit this multiphoton plateau are given in fig. 14a,b (see, also fig. 7). The differences in unperturbed energies $E_n = -1/2n^2$ between consecutive peaks of the distribution are equal to the field frequency; therefore, the sequence of peaks can be naturally explained as the result of a chain of one-photon transitions.

In the cases illustrated by fig. 14a,b these transitions start directly from the initial state n_0, and the peaks can be enumerated simply by the number of photons. However, the situation is not always that simple; in a series of cases, the chain of peaks does not start from n_0, but rather from somewhere inside the localized distribution (see fig. 2 in ref. [22]), and it is even possible to observe two or three distinct chains within the same distribution.

For the high-lying levels the heights of the peaks become roughly the same and they build up an equidistant (in energy) plateau. If we increase n still further, the peak heights do not decrease: this seems to be due to the fact that on high levels the field is strong enough for the probability of transitions between nearby peaks to be significant (saturated transitions). This is the second reason why $k_E < k_D$.

Upon increasing the field, the multiphoton plateau rises as a whole (fig. 14). The resonant peaks become broader, but in a number of cases they do not disappear, even in very strong fields and in the delocalization region. However, this usually takes place only for large ω_0 (compare delocalization in figs. 11a and 14b, for $n_0 = 100$, $\omega_0 = 1.5$ and 3, respectively).

In our opinion, the appearance of the multiphoton plateau below the ionization threshold is in its substance akin to the appearance of peaks in the energy distribution of photoelectrons which is observed above the ionization threshold [42, 43]. Indeed, for large n the distance between nearby levels is very small: $\Delta E \ll \omega$, and the spectrum in this region behaves like a quasi-continuum. It is then

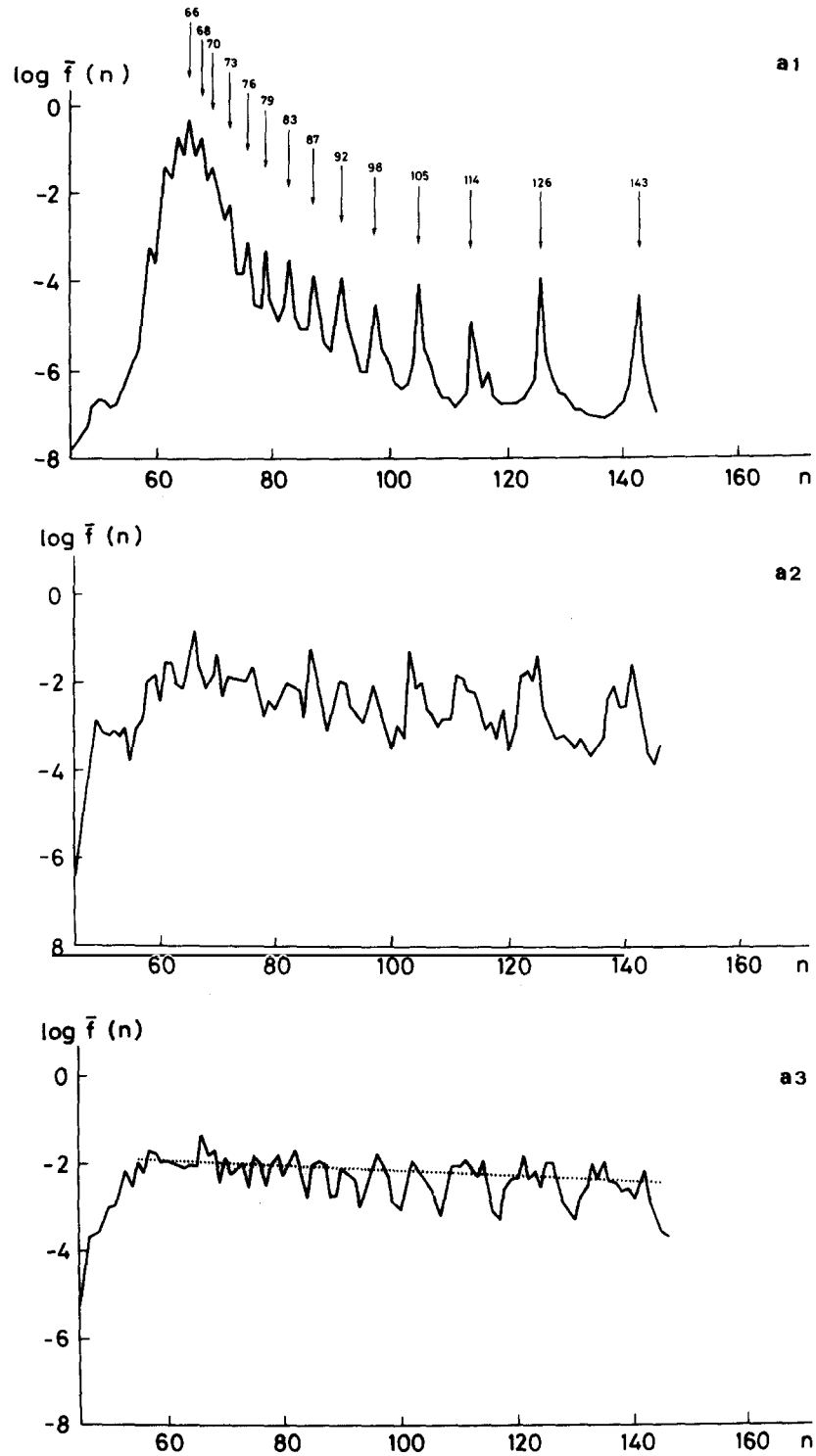

Fig. 14a. Quantum probability distribution $\bar{f}(n)$ averaged over 60 periods of τ within the interval $60 < \tau < 120$. Here $n_0 = 66$, $\omega_0 = 2$ and $\varepsilon_0 = 0.03$ (a1); $\varepsilon_0 = 0.08$ (a2); $\varepsilon_0 = 0.14$ (a3); the dotted line is the solution of the Fokker–Planck equation. The arrows with integers are the positions and principal quantum numbers of the peaks on the multiphoton plateau.

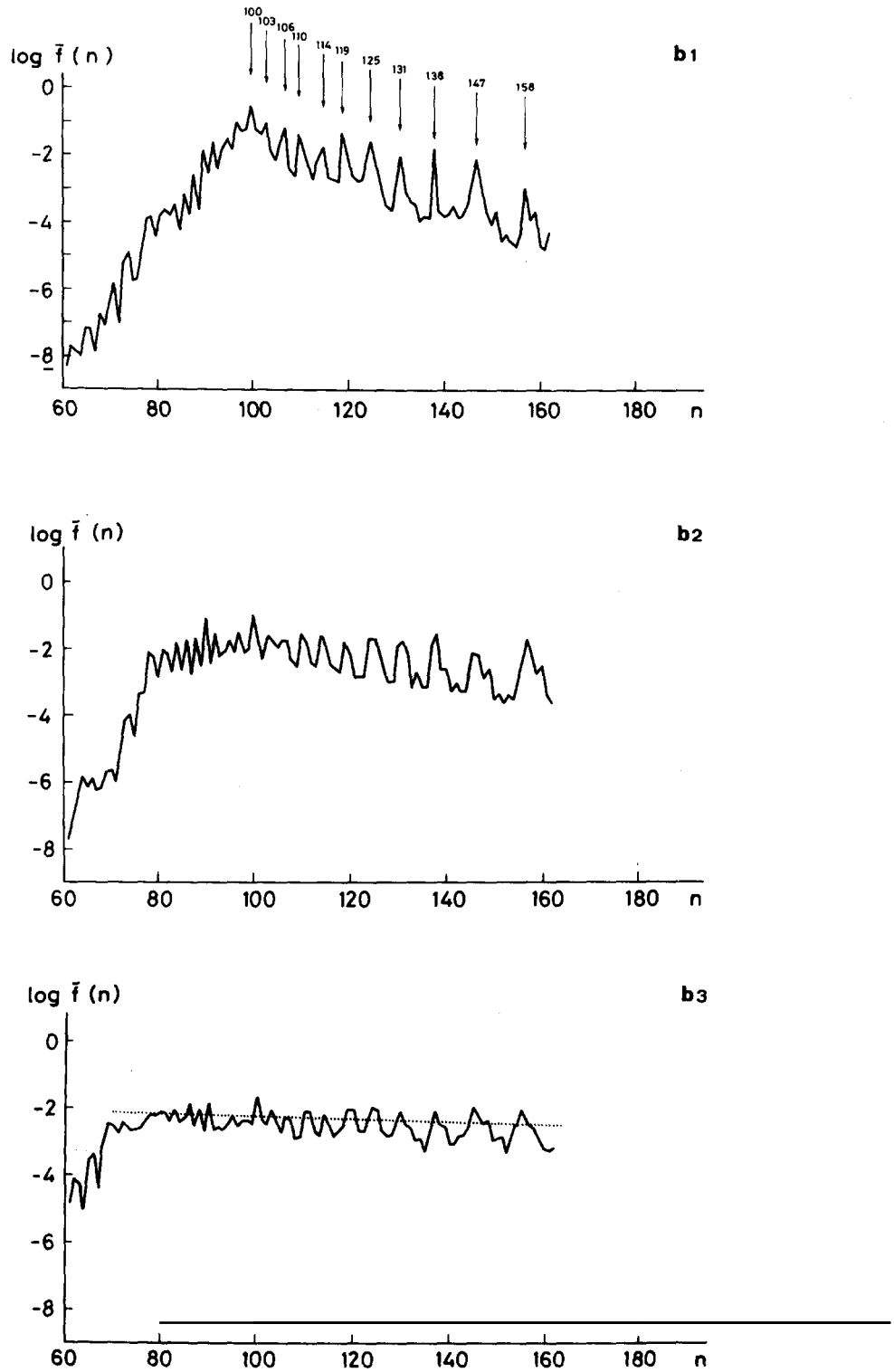

Fig. 14b. Same as fig. 14a with $n_0 = 100$, $\omega_0 = 3$ and $\varepsilon_0 = 0.06$ (b1); $\varepsilon_0 = 0.1$ (b2); $\varepsilon_0 = 0.2$ (b3).

reasonable to expect that the peak structure observed in the discrete part of the spectrum will persist also in the continuum.

It is possible that a theoretical explanation of the multiphotonic plateau in the underthreshold distribution may be given, along similar lines as in [44].

3.4. Dependence of the excitation probability on frequency

An example of the dependence of $W_{1.5}$ on ω_0 for fixed $\varepsilon_0 = 0.04$ and different n_0 is shown in fig. 15. It is here apparent that for high frequencies $\omega_0 > 1$ the excitation probability is significantly less than the corresponding classical one. The reason is that the delocalization threshold (15) increases with the frequency ω_0, so that a majority of points in fig. 15 belong to the region of localization. We recall, however, that the estimate (15) is only valid for $\omega_0 > 1$. Indeed, for $\omega_0 < 1$ a dynamical amplification in the classical excitation takes place, as described in section 3.2 (see fig. 5). From figs. 5, 15 it appears that for $\varepsilon_0 = 0.04$ the maximum classical excitation is gotten for $\omega_0 \approx 0.7$. Now, as is seen from fig. 15, the quantum probability of excitation for $n_0 = 30, 45, 66, 100$ is close to the classical value, and even the corresponding distributions on levels (fig. 16) look rather close to classical results. We interpret this fast

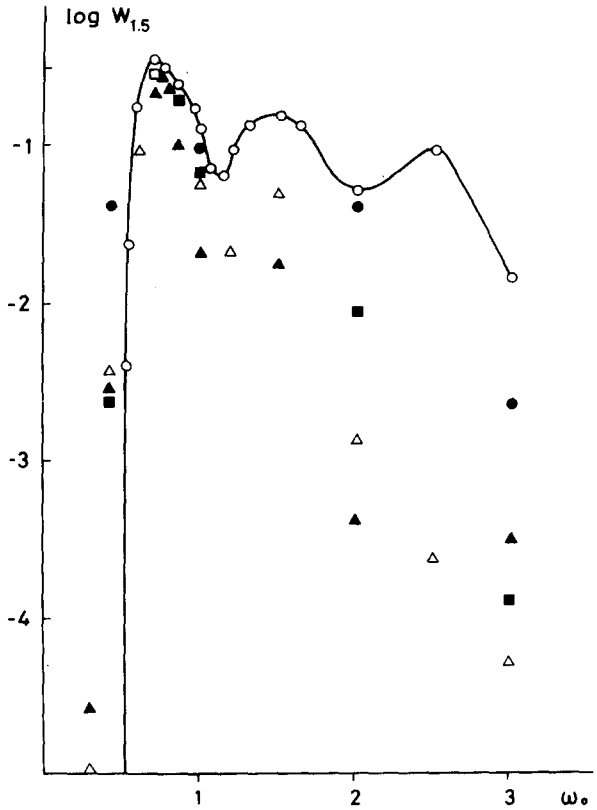

Fig. 15. Excitation probability $W_{1.5}$ as a function of frequency ω_0 at $\tau = 40\omega_0$ for fixed $\varepsilon_0 = 0.04$ and for different n_0. (●) $n_0 = 30$; (▲) $n_0 = 45$; (△) $n_0 = 66$; (■) $n_0 = 100$. The solid line, with open circles, gives the classical excitation probability. Notice that, by increasing ω_0, the quantum excitation probability becomes much less than the corresponding classical one due to the fact that the delocalization border (eq. (15)) increases with ω_0.

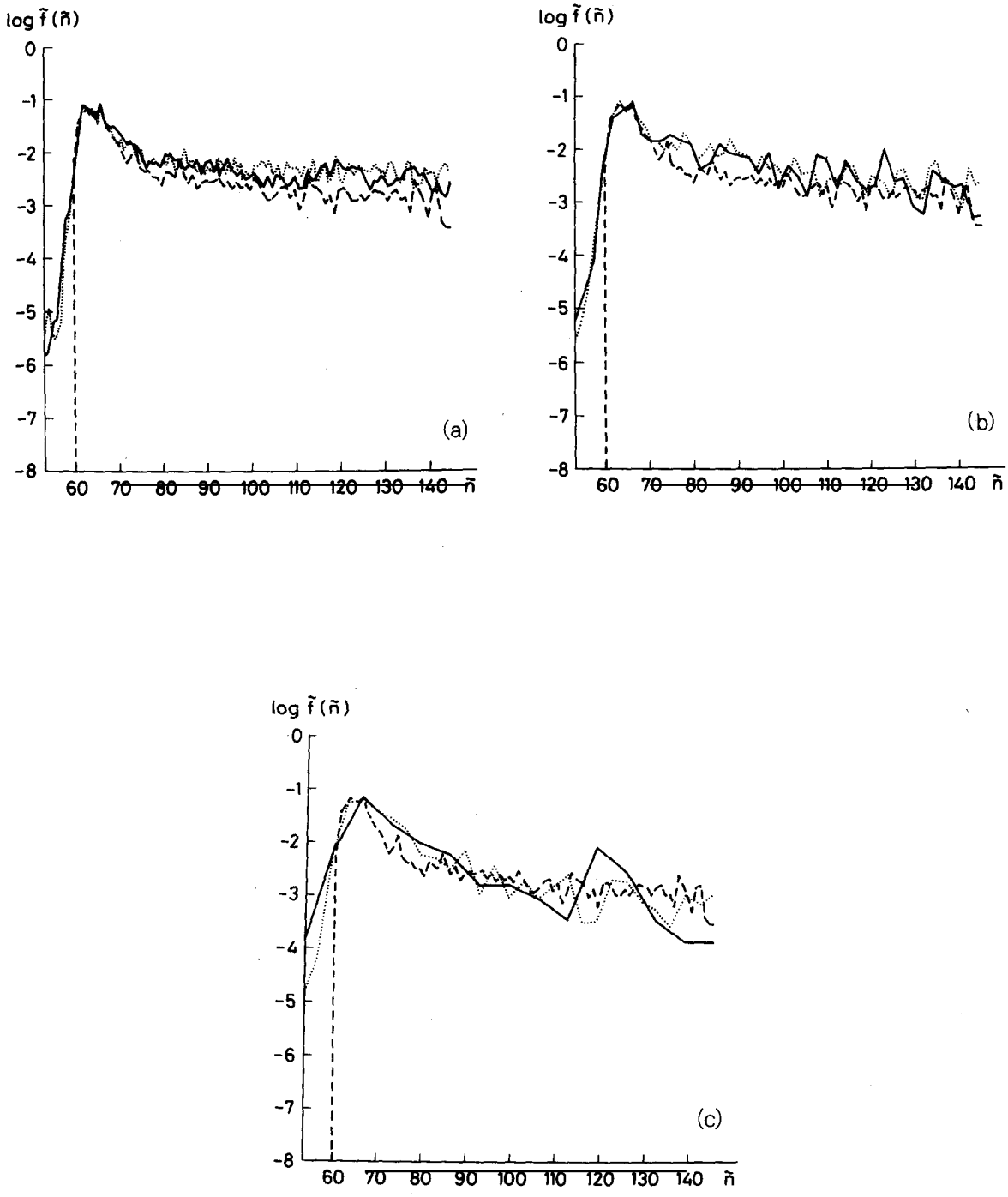

Fig. 16. Quantum probability distribution $\tilde{f}(\tilde{n})$ averaged over 40 periods of τ in the interval $40 < \tau < 80$ for fixed $\varepsilon_0 = 0.04$, $\omega_0 = 0.7$, and different n_0. (a) $n_0 = 100$ (dotted curve), $n_0 = 66$ (full curve); (b) $n_0 = 45$ (dotted curve), $n_0 = 30$ (full curve); (c) $n_0 = 20$ (dotted curve) $n_0 = 10$ (full curve). The classical probability distribution is also shown (dashed line). In order to compare the quantum distributions with different n_0, with the classical one, we have introduced rescaled quantities $\tilde{f} = (n_0/66)f$ and $\tilde{n} = (66/n_0)n$. The scaling property of the quantum distribution and the fairly good agreement with the classical motion is due to the delocalization phenomenon.

excitation in the sense that in the quantum system for this frequency there is a delocalization. Thus numerical experiments show that even for a rather weak field $\varepsilon_0 = 0.04$ delocalization can take place, nevertheless, at frequency $\omega_0 \approx 0.7$, lower than the Kepler frequency.

The fine structure of the dependence of excitation on frequency is shown in fig. 17. In the localization region $\omega_0 \approx 1$ one observes an essentially resonant dependence on frequency. For low frequencies $\omega_0 < 0.7$ most resonances disappear and the dependence on ω_0 becomes smoother. An analogous smoothing occurs in the region $\omega_0 \approx 1$, upon increasing n_0 from 30 to 100.

For still lower frequency, $\omega_0 < 0.6$, one falls into the region of classical stability; therefore, excitation ceases for the classical system. Then, the quantum excitation sharply diminishes, too. Thus, the dependence of the excitation probability on frequency has a threshold character, in that ionization takes place for

$$\omega_0 > \omega_c \sim 1 . \tag{36}$$

This estimate for the chaotic threshold ω_c is justified by the fact that for $\omega_0 < 1$ there are no 1st-order resonances between the frequency of the external field and the harmonics of the frequencies of the motion of the classical electron [18]; therefore, chaotic excitation for frequency $\omega_0 < 1$ can take place only for fields strong enough that higher-order resonances overlap. On the other hand, for very low frequency $\omega_0 \ll 1$ the value of the critical field ε_s coincides with that for the classical static field ionization. Notice that the threshold (36) holds only if $\varepsilon_0 > 1/50$. Otherwise, the chaotic threshold has to be determined from eq. (3), and is equal to $\omega_c \approx 1/(50\varepsilon_0)^3$.

According to the theoretical estimate (24), the diffusive ionization is more effective than direct one-photon ionization. In order to check this prediction we performed a series of numerical experiments, in which the ionization probability from states with $n_0 = 30$ or $n_0 = 66$ was investigated over a

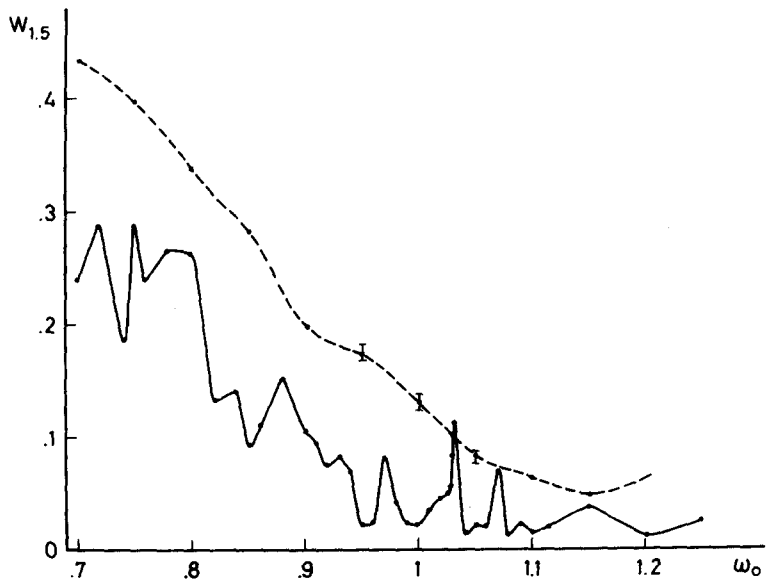

Fig. 17. Fine structure of the dependence of excitation probability $W_{1.5}$ on frequency ω_0 at $\tau = 40$ for fixed $\varepsilon_0 = 0.04$. $n_0 = 45$ (full curve); classical results (dashed curve).

broad range of frequencies. The field intensity was so chosen, that direct two-photon ionization was considerably less than 1-photon ionization except for intermediate resonances; moreover, $\varepsilon_0 < \varepsilon_s$, where ε_s is the critical intensity for static field ionization. In this situation, the photoeffect is expected to display a threshold dependence on frequency, with negligibly small ionization probability for $\omega_0 < \omega_\Phi = n_0/2$.

Such a picture of the photoeffect proved to be incorrect. In figs. 18, 19 we show the dependence on frequency of the probability of "ionization" W_I which we define as the excitation above a level $\bar{n}$ after a dimensionless time $\tau = 40\omega_0$ that corresponds to the same physical time for all ω_0's. Computations were made in the Sturm basis, so that W_I includes the probability of transition into the continuous spectrum. For $n_0 = 30$, we took $\bar{n} = 90$; and for $n_0 = 66$, $\bar{n} = 99$. Notice that W_I included some probability on discrete unperturbed levels, too. In figs. 18, 19 the most effective excitation is observed at frequencies well below the one-photon threshold. The new threshold value $\omega_c \sim 1$ is close to the corresponding classical value and, as explained above, is determined by the condition of overlapping of 2nd-order

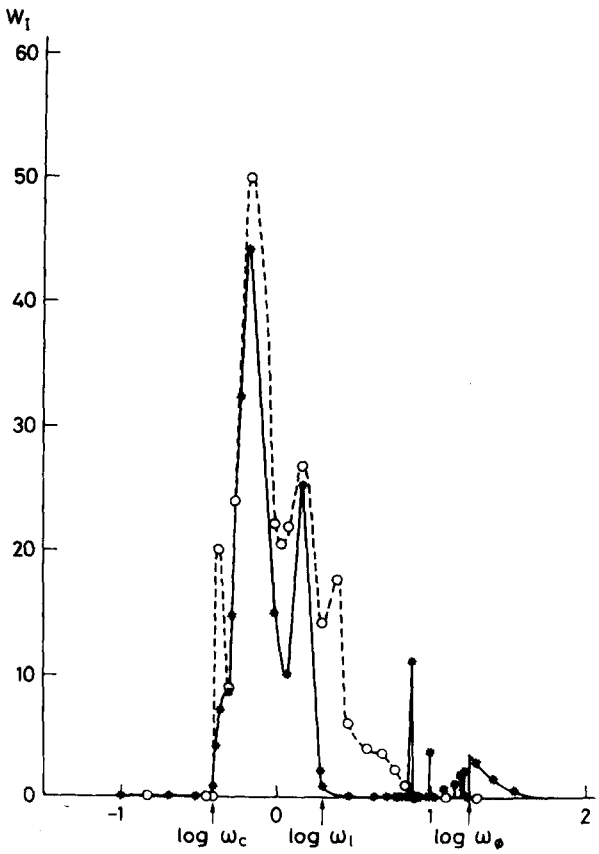

Fig. 18. Ionization probability $W_I = \Sigma_{n>\bar{n}} |c_n|^2$ versus field frequency ω_0 after a time $\tau = 40\omega_0$ which corresponds to the same physical time t for all frequencies. We have set $n_0 = 66$, $\varepsilon_0 = 0.05$, $\bar{n} = 99$. Moreover, quantum theory (*); classical theory (O). Notice that ω_Φ is here somewhat less than $n_0/2$ because, in our definition of the ionization probability, the contribution of states with $n > \bar{n}$ is also included.

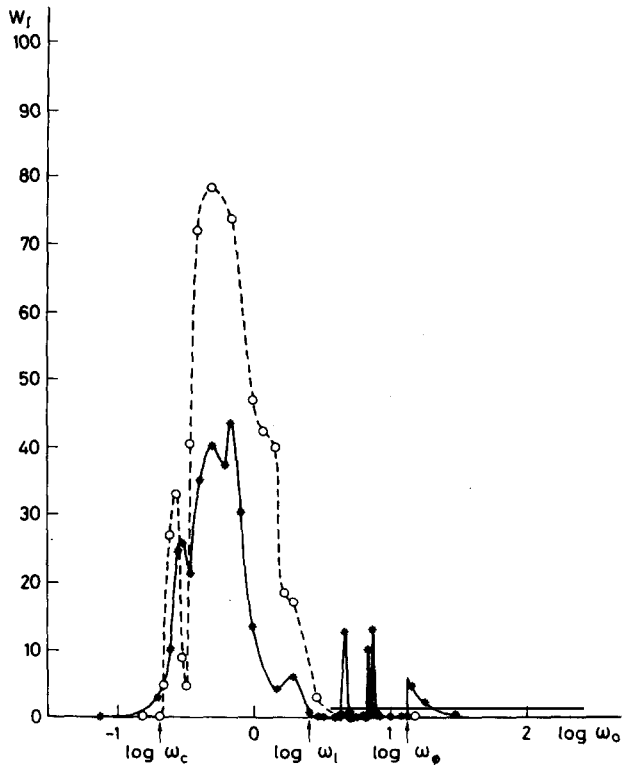

Fig. 19. Same as fig. 18 with $n_0 = 30$, $\varepsilon_0 = 0.075$, $\bar{n} = 90$.

resonances. For sufficiently strong field, ω_c appears to be significantly less than 1; for $\varepsilon_0 = 0.075$, $n_0 = 30$, the experimental value for ω_c is ≈ 0.2, and for $\varepsilon_0 = 0.05$, $n_0 = 66$ the threshold is $\omega_c \approx 0.35$.

In the quantum case, however, there is still a small probability of excitation even from the region $\omega_0 < \omega_c$, due to tunneling into the classically forbidden region. In the interval $\omega_c < \omega_0 < \omega_l = (6 n_0 \varepsilon_0^2)^{3/7}$ delocalization takes place, so that W_I is close to its classical value. For $\omega_l < \omega_0 < \omega_\Phi$ quantum effects lead to the localization of diffusion; therefore, in that region one observes an essentially different excitation picture than in the classical system. A decrease of W_I with ω_0 is observed also in the classical case, due to the decrease of the diffusion rate with ω_0 (see eq. (5)). Indeed, even in the presence of diffusion, the excitation probability above a given level n is nearly zero if at the given observation time τ the diffusion has not yet reached this n (i.e. if $\tau \ll (n - n_0)^2/D$). However, in the quantum case, isolated ionization spikes survive in this frequency region (see figs. 18, 19) due to transition into the continuum via intermediate resonant levels (compare with the multiphoton plateau in fig. 14a1).

In the frequency region $\omega_0 \approx \omega_\Phi$ the probability W_I sharply increases, because of the possibility of direct one-photon transitions. However, W_I in this region is significantly less than for $\omega_0 \sim 0.7$ when diffusive ionization occurs. In the region $\omega_0 > \omega_\Phi$ numerical data agree satisfactorily with the theoretical formula (22). This agreement is another indication that the Sturm basis method of integration efficiently describes continuous spectrum effects.

In fig. 18 we see that for $\omega_0 \approx 0.43$ the quantum probability of excitation is comparable with the classical one; again, this means that in this frequency region, for $n_0 = 66$, $\varepsilon_0 = 0.05$, there is quantum delocalization.

Numerical experiments indicate that the threshold value ε_{cr} for diffusive excitation in this frequency region lies between 0.04 and 0.05 (fig. 5). In the quantum case, upon varying ε_0 from 0.04 to 0.05 the excitation probability changes by about two orders of magnitude. This means that delocalization occurs already at $\varepsilon_0 \approx \varepsilon_{cr}$, so that the field strength yielding 10% ionization (which was studied in ref. [26]) will be found to agree with classical predictions. In other words, these numerical experiments of ours show that laboratory experiments [13, 27] were performed in that parameter region where one-dimensional delocalization (and a fortiori two-dimensional delocalization) takes place, and this explains the observed agreement with predictions from the classical model.

3.5. Stability of quantum diffusion

Even though the diffusive ionization, taking place in the delocalization regime, is to some extent similar to the classical diffusion which occurs in the chaotic regime, the quantum system is still short of exhibiting all the statistical properties that would be expected of classical chaos.

The most striking difference is the absence, in quantum dynamics, of the strong instability and of the rapid loss of memory associated with classical chaos. In computer experiments this effect leads to irreversibility. Indeed, even though the exact equations of motion are reversible, nevertheless any, however small, imprecision in solving them, such as computer round-off errors, is magnified by the exponential instability of orbits to the extent that initial conditions are effaced and reversibility is therefore destroyed.

Investigations aimed at verifying whether an analogous irreversibility would also be displayed by the numerically computed quantum evolution were described in [6] for the kicked rotator. Here we will present numerical results for time-reversal experiments on the one-dimensional H-atom (figs. 11, 12). The chosen parameter values lie in the region of delocalization; therefore, up to the moment of time-reversal ($\tau = 60$) diffusive excitation is going on, both in the quantum and in the classical system.

Indeed, the distribution on the quantum levels at $\tau = 60$ is close to the classical one, and is well described by formula (5a). Then, at $\tau = 60$ we reversed the velocities of all particles ($N = 1000$) in the classical ensemble, and changed the wave function of the quantum atom to its complex conjugate. In both classical and quantum mechanics, the H-atom would be expected to find its way back to the initial state. However, due to the finite computer precision, in the classical case such a return is not observed. The system retraces backward its history just for a few periods of the field, and then, again, diffusive excitation occurs.

Instead, in the quantum case an almost exact reversion of motion is gotten; at time $\tau = 120$ the electron comes back to the initial level. This is even more remarkable on account of the fact that, in order to restore the initial state, some of the total probability had to be called back from the continuum.

The conclusion must be drawn from this exact reversibility, that even though the quantum diffusion which occurs in the delocalization regime of the H-atom is by now the most chaotic example of quantum motion hitherto investigated, nevertheless this quantum "chaos" is essentially different from the real chaos of classical dynamics.

4. Experimental results

A large number of laboratory experiments on hydrogen and alkali atoms in highly excited states have been performed up to now [13, 14, 23–27]. Additional interest for such experiments has recently arisen in connection with the possibility of chaotic motion in quantum mechanics. It is now possible to perform experiments on microwave ionization on atoms prepared in extended quasi-one-dimensional states [24]. Here it is possible to measure the ionization probability identified with the population of levels higher than some sufficiently large n, including the continuum; this definition is particularly convenient for comparison with numerical experiments. Also, it is possible to measure the probability distribution on unperturbed levels. This allows, in principle, for a careful comparison of experimental and numerical data.

In particular, very accurate experiments on one-dimensional H-atoms were carried through as described in [24]. Also extensive experimental data on extended atoms in combined static and microwave fields are presented in [54]. The range of parameters for these experiments lies inside the region of low frequency ($\omega_0 \approx 0.2$) and of classical stability (see also [28]), so that the results can not be used as a test for the theory presented in this paper.

A different series of experiments [27] was performed on two-dimensional H-atoms. The conditions of these experiments not only lie above the two-dimensional delocalization border, but even above the one-dimensional one. For this reason, our results predict an agreement with classical computations, as indeed was found in [27]. One possible explanation for the not complete agreement obtained is that the experimental values in [27] might be above but close to the delocalization border, when one should not expect a better agreement than within a factor 2. To clarify this point we show in fig. 20 the comparison of numerical one-dimensional quantum and classical ionization probability slightly above the border: there is a strong excitation in both cases, but, unlike strongly delocalized cases (see, e.g., fig. 12) here the two results only agree within a 50%.

Since experimental techniques allow for very accurate measurements, it is highly desirable that the conditions of the experiments be defined as precisely as possible; for example it is more convenient to choose a single excited state than a microcanonical distribution. From our point of view, a most

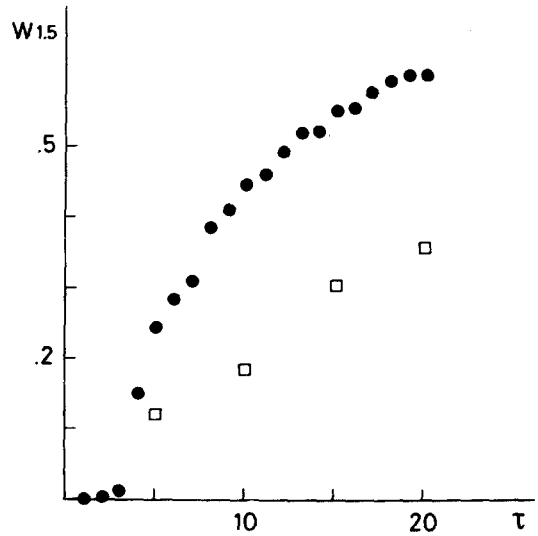

Fig. 20. Classical (●) and quantum (□) excitation probability as a function of time for $n_0 = 66$, $\varepsilon_0 = 0.06$, $\omega_0 = 0.43$. The quantum system is delocalized but since we are only slightly over the border, the quantum excitation is less than the classical one.

important goal for future experiments is to observe and to study the new and unexpected localization phenomenon in classically chaotic situations. For this it is necessary that the frequency ω_0 be increased above $\omega_0 \approx 1$, since in the region $\omega_0 > 1$ a large separation between the classical chaotic threshold ω_c and the quantum delocalization border ω_l is expected. In the high frequency region it is also possible, by varying the field strength, to observe the transition to delocalization as well as the other phenomena described in the present paper.

Also, in order to give experimental evidence for the "freezing" of the wave packet in localization, it would be desirable to vary the interaction time. This latter possibility lies within the capabilities of present day technique [25].

We would like also to stress that all the phenomena described in this paper should be observable not only in H-atoms, but also in different alkali atoms. In order to produce hydrogen-like states in such atoms, one should take into account that, the unperturbed spectrum for highly-excited alkali atoms is slightly different than in H-atoms, due to the quantum defect. However, for values of $l > 3$ this quantum defect is negligible. Since in linearly polarized fields the magnetic quantum number m is a constant of the motion, by exciting states with $m \geq 3$ it is possible to excite states with $l \geq 3$, which correspond very well to the hydrogenic situation. It is then possible to consider also one-dimensional problems for levels with $m \geq 3$, $n_2 = 0$, $n_1 = n - |m| - 1$ and this excitation can be achieved via light-induced resonant transitions. One would then get a situation in which localization and other effects of quantum chaos might be studied.

5. Conclusions

The study of the one-dimensional H-atom in a monochromatic field that we have described in the present paper brings to light a number of facts – some of which were rather unexpected.

These facts concern both the actual physics of atoms in microwave fields, and the general problem of quantum dynamics in the region of classically chaotic motion. Even though the unperturbed eigenfunc-

tions, as well as the matrix elements of the perturbation, can be well approximated by their semiclassical expressions, it may well happen that quantum and classical time evolutions are essentially different, due to the phenomenon of quantum localization of chaos. It is interesting to note that investigations of this phenomenon were prompted by studies on the rotator model [4]. It is a remarkable fact that this phenomenon, originally detected in a somewhat artificial model, has now been shown to exist in a physical system, so that there is a real possibility to observe it in laboratory experiments.

On the other hand, for the H-atom a delocalization regime also exists, and our theory allows determination of the threshold for this regime. Above this threshold, the excitation of the quantum system can be approximately described by the classical diffusive excitation. This regime of excitation is much more efficient than the direct 1-photon ionization; therefore a new frequency threshold for the photoelectric effect appears, which is determined by the classical border for frequency, $\omega_0 > \omega_c$. Actually there are two different frequency thresholds ω_c and ω_l, so that strong ionization occurs only for $\omega_c < \omega_0 < \omega_l$. The latter threshold ω_l is due to quantum localization of classical chaos.

The delocalization phenomenon explains the partial success of classical computations in reproducing experimental results on microwave ionization. At the same time, however, the localization phenomenon sets definite limits to the applicability of classical models, which are due to quantum localization.

Although a discussion of the two-dimensional case was given in section 2.2, the bulk of the results presented in this paper were related to the one-dimensional case. While this fact does not affect the conceptual importance of these results, it enforces some caution when comparing them with experiments hitherto performed. Indeed, an analysis of the experiments described in [48] shows that a two-freedoms theory is required to model them properly.

Delocalization is also a challenging subject for future theoretical analysis. This phenomenon has been predicted on the grounds of semiclassical arguments, which are best suited to make contact with classical chaotic behavior. Nevertheless, it should be possible to understand it in purely quantum terms.

A few concluding remarks are in order concerning the relationship of results described in this paper to the general themes of quantum chaos. As we have seen, diffusive excitation and ionization are brought about in the classical hydrogen atom by the onset of dynamical chaos, which is a regime of extreme instability of trajectories of the electron. A physically relevant question that we have answered above, is whether the physically observable manifestations of chaos – enhanced ionization and so on – survive also in the quantum domain. However, the more speculative question may be posed, whether also anything of the conceptual setup of classical chaos – instability, irreversibility, and so on – can be translated in a quantum context. An illustration was given in this paper (section 3.5) that this is not the case. However similar the quantum evolution may appear to the classical one (insofar as the population of levels is concerned) it remains strongly stable, in sharp contrast to the latter. Therefore, even though classical chaos was shown to be relevant in predicting the response of a quantum hydrogen atom to an external microwave field, it must be stressed again that, strictly speaking, no true chaos is possible in quantum mechanics.

Acknowledgments

We thank R. Bonifacio, J. Ford, F.M. Izrailev, G. Mantica and L. Perotti for stimulating discussions. This work was performed with the support of the Consiglio Nazionale delle Ricerche (Italy).

Appendix I: Quasi-classical matrix elements in parabolic coordinates

We shall here get the expression for the z coordinate in parabolic action–angle variables $(n_1, n_2, m, \lambda_1, \lambda_2, \varphi)$. To this end we introduce the parabolic coordinates ξ, η, φ:

$$\begin{aligned} x &= (\xi\eta)^{1/2}\cos\varphi \\ y &= (\xi\eta)^{1/2}\sin\varphi \\ z &= (\xi-\eta)/2\,. \end{aligned} \tag{I.1}$$

In these coordinates the unperturbed Hamiltonian takes the form:

$$H = 2\xi P_\xi^2/(\xi+\eta) + 2\eta P_\eta^2/(\xi+\eta) + P_\varphi^2/(2\xi\eta) - 2/(\xi+\eta)\,. \tag{I.2}$$

The transformation to action–angle variables $(n_1, n_2, m, \lambda_1, \lambda_2, \varphi)$ is achieved by separation of variables in the Hamilton–Jacobi equation for which we refer to standard textbooks (see e.g. [31]). Here we just recall that the generating function of this transformation is found to be:

$$S(n_1, n_2, m, \xi, \eta, \varphi) = \int^{\xi} P_\xi\, \mathrm{d}\xi' + \int^{\eta} P_\eta\, \mathrm{d}\eta' + m\varphi \tag{I.3}$$

where the canonical momenta P_ξ, P_η, P_φ are given by [29, 31]:

$$\begin{aligned} P_\xi &= [E/2 + \beta_1/\xi - m^2/4\xi^2]^{1/2} \\ P_\eta &= [E/2 + \beta_2/\eta - m^2/4\eta^2]^{1/2} \\ P_\varphi &= m \\ \beta_{1,2} &= (n_{1,2} + |m|/2)/n\,, \qquad n = n_1 + |m|\,, \qquad E = -1/2n^2\,. \end{aligned}$$

Then the angle variables λ_1, λ_2

$$\lambda_{1,2} = \partial S/\partial n_{1,2} \tag{I.4}$$

can be obtained by differentiating (I.3) and computing the integrals. The procedure is greatly simplified by the introduction of the auxiliary angles χ_1, χ_2 defined by

$$\begin{aligned} \xi &= -2n^2\mu_1\sin\chi_1 + 2n(n_1 + |m|/2) \\ \eta &= -2n^2\mu_2\sin\chi_2 + 2n(n_2 + |m|/2)\,, \end{aligned} \tag{I.5}$$

where the parameters μ_1, μ_2 are given by:

$$\mu_{1,2} = [n_{1,2}(n - n_{2,1})/n^2]^{1/2} .$$

In this way we get the following result:

$$\begin{aligned} \lambda_1 &= -\mu_1 \cos \chi_1 - \mu_2 \cos \chi_2 - \chi_1 + \pi/2 \\ \lambda_2 &= -\mu_1 \cos \chi_1 - \mu_2 \cos \chi_2 - \chi_2 + \pi/2 . \end{aligned} \tag{I.6}$$

From (I.5) we get the following expression for z:

$$z = \tfrac{1}{2}(\xi - \eta) = n^2(\mu_2 \sin \chi_2 - \mu_1 \sin \chi_1) + n(n_1 - n_2) . \tag{I.7}$$

The coordinate z can be expanded in a double Fourier series in the angles λ_1, λ_2 with coefficients $z_{k_1 k_2}$ given by:

$$z_{k_1 k_2} = \int \mathrm{d}\lambda_1 \int \mathrm{d}\lambda_2 \, z \exp\{-\mathrm{i}(k_1\lambda_1 + k_2\lambda_2)\} .$$

We now substitute (I.7) for z in this integral, and change integration variables to χ_1, χ_2 by using (I.6). Thus we find:

$$z_{k_1 k_2} = n^2 \int_0^{2\pi} \mathrm{d}\chi_1 \int_0^{2\pi} \mathrm{d}\chi_2 \, D(\chi_1\chi_2)(\mu_2 \sin \chi_2 - \mu_1 \sin \chi_1) \exp\{-\mathrm{i}(k_1\lambda_1 + k_2\lambda_2)\} + n(n_1 - n_2)\delta_{0k_1}\delta_{0k_2} \tag{I.8}$$

where $D(\chi_1, \chi_2) = \partial(\lambda_1, \lambda_2)/\partial(\chi_1, \chi_2) = 1 - \mu_1 \sin \chi_1 - \mu_2 \sin \chi_2$ is the Jacobian determinant for the transformation $(\lambda_1, \lambda_2) \to (\chi_1, \chi_2)$.

Evaluating the double integral in (I.8) yields formulas (1d) in the text.

Appendix II: Solution of the Fokker–Planck equation

In order to solve eq. (4) with the boundary condition $\partial f/\partial n|_{n=n^*} = 0$, we shall first perform some change of variables. First of all, putting $\bar{\tau} = \varepsilon_0^2 \tau/\omega_0^{7/3}$, $y = n/n_0$, the Fokker–Planck equation takes the form:

$$\partial f(y, \bar{\tau})/\partial\bar{\tau} = \partial/\partial y(y^3 \, \partial f/\partial y) .$$

Now let's change again variables to $z = y^{-1/2}$ and let's introduce a new function $g(z, \bar{\tau})$ according to $f = z^2 g$. This function g must then satisfy:

$$\partial g/\partial\bar{\tau} = \tfrac{1}{4} \, \partial^2 g/\partial z^2 + (1/4z) \, \partial g/\partial z - (1/z^2)g$$

and its Laplace transform $\tilde{g}(z, s)$ must satisfy the equation:

$$\partial^2\tilde{g}/\partial z^2 + (1/z)\,\partial\tilde{g}/\partial z - (4/z^2 + 4s)\tilde{g} = -4g(z,0)\,.$$

A further change of variables to $x = 2z\sqrt{s}$ yields:

$$\partial^2\tilde{g}/\partial x^2 + (1/x)\,\partial\tilde{g}/\partial x - (1 + 4/x^2)\tilde{g} = -(1/s)\,g(x,0)\,. \tag{II.1}$$

By the same changes of variables we find that, in order that f satisfies the boundary condition $\partial f/\partial n|_{n=n^*} = 0$, $\tilde{g}$ must satisfy:

$$\partial\tilde{g}(x,s)/\partial x|_{x=\bar{x}} = -(2/x)\,\tilde{g}(\bar{x},s)\,, \qquad \text{where } \bar{x} = 2(sn_0/n^*)^{1/2}\,. \tag{II.2}$$

The general integral of eq. (II.1) can be written as

$$\tilde{g} = A\,I_2(x) + B\,K_2(x) + \bar{g}$$

where I_2, K_2 are modified Bessel functions; A, B are numerical constants and $\bar{g}$ is a particular integral that can be determined, e.g. by Lagrange's method:

$$\tilde{g} = I_2(x)\left[A - (1/s)\int_0^x x'\,g(x',0)\,K_2(x')\,\mathrm{d}x'\right] + K_2(x)\left[B + (1/s)\int_0^x x'\,g(x',0)\,I_2(x')\,\mathrm{d}x'\right]. \tag{II.3}$$

The constants A, B can then be chosen so that the boundary condition (II.2) is satisfied. Indeed, upon substituting (II.3) into (II.2) we get:

$$\tilde{g}(x,s) = [K_1(\bar{x})\,I_2(x)/I_1(\bar{x})]\,(1/s)\int_0^{\bar{x}} g(x',0)\,I_2(x')\,x'\,\mathrm{d}x'$$

$$+ I_2(x)\,(1/s)\int_x^{\bar{x}} g(x',0)\,K_2(x')\,x'\,\mathrm{d}x' + K_2(x)\,(1/s)\int_0^x g(x',0)\,I_2(x')\,x'\,\mathrm{d}x'\,. \tag{II.4}$$

Since $f(n,0) = \delta(n - n_0)$, we must choose $g(x,0)$ in the form $\delta(4s/x^2 - 1)$. Then the asymptotics of (II.4) for $s\to\infty$ and fixed y has the form:

$$g(x,s) \sim (4s/x^2)^{1/4}\,(1/2\sqrt{s})\,\{\exp[2\sqrt{s}(1 + x/2\sqrt{s} - \bar{x}/2\sqrt{s})] + \exp[2\sqrt{s}\,(x/2\sqrt{s} - 1)]\}$$

whence it follows

$$\tilde{f}(y,s) \underset{s\to\infty}{\sim} (1/2y^{3/4}\sqrt{s})\,\{\exp[2\sqrt{s}\,(1 + 1/\sqrt{y} - 2/\sqrt{\bar{y}})] + \exp[2\sqrt{s}\,(1/\sqrt{y} - 1)]\}\,.$$

Equation (5a) in the text easily follows from the last formula.

Appendix III: Estimate for the delocalization border

Let's evaluate the 2nd moment of the distribution over the levels: $M_2 = \langle (\Delta n)^2 \rangle = \langle (n - \langle n \rangle)^2 \rangle$. From the diffusion equation we get approximately

$$\mathrm{d}/\mathrm{d}\tau \langle (\Delta n)^2 \rangle \approx \langle D \rangle = a n_0^2 \langle (n/n_0)^3 \rangle \tag{III.1}$$

where $a = 2\varepsilon_0^2 \omega_0^{-7/3}$. The equation for the 1st moment gives

$$\mathrm{d}\langle n \rangle / \mathrm{d}\tau = (3an_0/2)\langle (n/n_0)^2 \rangle \,. \tag{III.2}$$

In order to solve (III.1) and (III.2) we will use a rough approximation, namely, we will substitute for n its mean value $\langle n \rangle$ which is justified if the localization length $l \ll n_0$. Doing so, and performing the integration, we obtain

$$\langle n \rangle = n_0 [1 - 3a\tau/2]^{-1}$$

$$\langle (\Delta n)^2 \rangle = n_0^2 [(1 - 3a\tau/2)^{-2} - 1]/3 \,.$$

The localization condition $\tau^2 = \alpha^2 \langle (\Delta n)^2 \rangle = \alpha^2 l^2$ gives an equation for τ, the least root of which determines the localization length l:

$$\begin{aligned} &(n_0^2/3)[(1 - 3\tau a/2)^{-2} - 1] = \tau^2/\alpha^2 \\ &l = \tau/\alpha \,. \end{aligned} \tag{III.3}$$

A straightforward manipulation gives then formulas (13), (14) with $u = 3\tau a/2$.

Appendix IV: A method for computing hypergeometric functions

The numerical computations of matrix elements in (35) presents some technical difficulty since a direct expansion of hypergeometric functions in power series of $-4nn_0/(n - n_0)^2$ doesn't give correct values of B_{ns} for $n \sim s \sim 100$ due to strong cancellations of different terms and finite computer precision. Therefore in order to compute the hypergeometric function F we used a different method based on the recursion formulas between values of F for three consecutive values $s - 1$, s, $s + 1$ (see, e.g. [40]). The method is essentially as follows:

We take two exact values of $F(-s, -(n-1), 2, z)$ for $s = 0$, $s = 1$ ($F(s = 0) = 1$, $F(s = 1) = 1 + (n - 1)z/2$) and then we recurrently determine all F_s up to $s = n_s \approx n$. Since F_s increases from $s = 0$ up to $s = n_s \approx n$ and then decays up to $s = \infty$, the above procedure gives correct values of F_s only up to $s = n_s$. In order to compute F_s for greater values of s in a range $n_s < s < s_{\max}$ we take two arbitrary values for F_m and F_{m+1} where $m \gg s_{\max}$ (for example $m \approx 5s_{\max}$) and recurrently determine values of F for $n_s - 10 < s < m$. This latter procedure gives correct values of F up to an unknown constant C_F. The value of this constant is obtained by comparison with one of the previously computed F_s for $s < n_s$. The difference in the values of C_F thus obtained is less than 10^{-10}, which guarantee the correctness of the

method. After taking into account this constant factor we obtain very precise values for all F_s with $0 < s < s_{\max}$ (which obviously do not depend on the abritrary values F_m, F_{m+1}). An additional check is obtained by comparing the recurrent and the expansion method in regions where they work both (for example for $n \approx 30$).

References

[1] Proc. Int. Conf. on Quantum Chaos, Como 1983, ed. G. Casati (Plenum, 1985).
[2] G.M. Zaslavsky, Phys. Reports 80 (1981) 157.
[3] B.V. Chirikov, F.M. Izrailev and D.L. Shepelyansky, Sov. Sci. Rev. 2C (1981) 209.
[4] G. Casati, B.V. Chirikov, J. Ford and F.M. Izrailev, Lecture Notes in Physics (Springer) 93 (1979) 334.
[5] B.V. Chirikov, Phys. Reports 52 (1979) 263.
[6] D.L. Shepelyansky, Physica 8D (1983) 208.
[7] T. Hogg and B.A. Huberman, Phys. Rev. Lett. 48 (1982) 711.
[8] S. Fishman, D.R. Grempel and R.E. Prange, Phys. Rev. Lett. 49 (1982) 509; Phys. Rev. A 29 (1984) 1639.
[9] B.V. Chirikov, Usp. Fiz. Nauk 139 (1983) 360.
[10] B.V. Chirikov and D.L. Shepelyansky, Preprint 85-29, INP, Novosibirsk, 1985; Radiofizika 29 (1986) 1041.
[11] D.L. Shepelyansky, Phys. Rev. Lett. 56 (1986) 677.
[12] G. Casati and I. Guarneri, Commun. Math. Phys. 95 (1984) 12.
[13] J.E. Bayfield and P.M. Koch, Phys. Rev. Lett. 33 (1974) 258.
[14] J.E. Bayfield, L.D. Gardner and P.M. Koch, Phys. Rev. Lett. 39 (1977) 76.
[15] N.B. Delone, B.A. Zon and V.P. Krainov, Zh. Eksp. Teor. Fiz. 75 (1978) 445.
[16] J.G. Leopold and I.C. Percival, Phys. Rev. Lett. 41 (1978) 944; J. Phys. B 12 (1979) 709.
[17] B.I. Meerson, E.A. Oks and P.V. Sasorov, Pis'ma Zh. Eksp. Teor. Fiz. 29 (1979) 79.
[18] N.B. Delone, V.P. Krainov and D.L. Shepelyansky, Usp. Fiz. Nauk 140 (1983) 335 [Sov. Phys. Usp. 26 (1983) 551].
[19] D.L. Shepelyansky, Preprint 83-61, INP, Novosibirsk, 1983; Proc. Int. Conf. on Quantum Chaos, Como 1983 (Plenum, 1985) p. 187.
[20] R.V. Jensen, Phys. Rev. Lett. 49 (1982) 1365.
[21] R.V. Jensen, Phys. Rev. A 30 (1984) 386.
[22] G. Casati, B.V. Chirikov and D.L. Shepelyansky, Phys. Rev. Lett. 53 (1984) 2525.
[23] J.E. Bayfield, L.D. Gardner, Y.Z. Gulkov and S.D. Sharma, Phys. Rev. A 24 (1981) 138.
[24] J.E. Bayfield and L.A. Pinnaduwage, Phys. Rev. Lett. 54 (1985) 313; J. Phys. B 18 (1985) L49;
J.N. Bardsley, J.E. Bayfield, L.A. Pinnaduwage and B. Sundaram, Phys. Rev. Lett. 56 (1986) 1007.
[25] D. Meschede, H. Walter and G. Mueller, Phys. Rev. Lett. 54 (1985) 551.
[26] H. Rinneberg, J. Neukammer, G. Joensson, H. Hieronymus, A. Koenig and K. Vietzke, Phys. Rev. Lett. 55 (1985) 382.
[27] K.A.H. van Leeuwen, G.V. Oppen, S. Renwick, J.B. Bowlin, P.M. Koch, R.V. Jensen, O. Rath, D. Richards and J.G. Leopold, Phys. Rev. Lett. 55 (1985) 2231.
[28] R.V. Jensen, Phys. Rev. Lett. 54 (1985) 2057.
[29] L.D. Landau and E.M. Lifshitz, Quantum Mechanics (Moscow, Nauka, 1974).
[30] J.G. Leopold and D. Richards, J. Phys. B 18 (1985) 3369.
[31] L.D. Landau and E.M. Lifshitz, Mechanics (Moscow, Nauka, 1973).
[32] J.N. Bardsley and B. Sundaram, Phys. Rev. A 32 (1985) 689.
[33] L.D. Landau and E.M. Lifshitz, Field Theory (Moscow, Nauka, 1973) p. 236.
[34] S.P. Goreslavsky, N.B. Delone and V.P. Krainov, Zh. Eksp. Teor. Fiz. 82 (1982) 1789; preprint PhIAN USSR N33, Moscow, 1982.
[35] L.V. Keldysh, Zh. Eksp. Teor. Fiz. 47 (1964) 1945 [Sov. Phys. JEPT 20 (1965) 1307].
[36] E.V. Shuryak, Zh. Eksp. Teor. 71 (1976) 2039.
[37] R. Blumel and U. Smilansky, Phys. Rev. A 32 (1985) 1900.
[38] A.K. Dhar, F.M. Izrailev and M.A. Nagarajan, Preprint 83-162, INP, Novosibirsk, 1983.
[39] R. Blumel and U. Smilansky, Phys. Rev. Lett. 52 (1984) 137; Phys. Rev. A 30 (1984) 1040.
[40] H. Bateman and A. Erdelyi, Higher Transcendental Functions Vol. 1 (New York, McGraw-Hill Book Company, Inc., 1953).
[41] D.A. Jones, J.G. Leopold and I.C. Percival, J. Phys. B 13 (1980) 31.
[42] F. Fabre, G. Petite, P. Agostini and M. Clement, J. Phys. B 15 (1982) 1353.
[43] P. Kuit, J. Kimiman, H.G. Muller and M.J. van der Wiel, Phys. Rev. A 28 (1983) 248.
[44] Z. Deng and J.H. Eberly, Phys. Rev. Lett. 53 (1984) 1810.
[45] D.E. Khmelnitskii, Pis'ma Zh. Eksp. Teor. Fiz. 32 (1980) 248.

[46] G. Casati, B.V. Chirikov, I. Guarneri and D.L. Shepelyansky, Phys. Rev. Lett. 57 (1986) 823.
[47] G. Casati, B.V. Chirikov, I. Guarneri and D.L. Shepelyansky, Phys. Rev. Lett. 56 (1986) 2437.
[48] P.M. Koch, in: Fundamental aspects of quantum theory, eds. V. Gorini and A. Frigerio (Plenum Press, 1987).
[49] R. Blumel and U. Smilansky, Phys. Rev. Lett. (to appear);
J.N. Bardsley, J.E. Bayfield, L.A. Pinnaduwage and B. Sundaram, Phys. Rev. Lett. 56 (1986) 1007.
[50] R. Blumel and U. Smilansky, preprint, 1986.
[51] J.N. Bardsley and M.J. Comella, J. Phys. B19L (1986) 565.
[52] Shortly before the definitive redaction of this paper, some new papers appeared in preprint form, reporting about further computational efforts in this sense [49, 50].
[53] J.G. Leopold and D. Richards, J. Phys. B19 (1986) 1125; The effect of a combined static and microwave field on an excited hydrogen atom (1986).
[54] J.E. Bayfield, in: Fundamental Aspects of Quantum Theory, eds. V. Gorini and A. Frigerio (Plenum Press, New York, 1986).